Food Chemistry: X 28 (2025) 102592

Contents lists available at ScienceDirect

Food Chemistry: X

journal homepage: www.sciencedirect.com/journal/food-chemistry-x

# Comprehensive analysis through multi-omics integration to compare and elucidate the specific substances in milk of donkey、horse、camel、human and pig

Qiu Zhang [1], Qian Li [1], Xiaowei Wang [1], Yanzhi Wu, Rui Chen, Yinggang Sun, Yuan Pan, Siyi Li, Zeying Wang [*]

*College of Animal Science & Veterinary Medicine, Shenyang Agricultural University, Shenyang 110866, China*

ARTICLE INFO

*Keywords:*
Lipidomics
Metabolomics
Proteomics
Phospholipid
Nicotinamide adenine dinucleotide
Albumin

ABSTRACT

Featured milk generally refers to less common dairy products with unique sources or specific nutritional components and functional characteristics. We used omics methods to study the lipids, metabolites, and proteins in donkey milk, mare milk, and camel milk and compared them with human milk and pig milk. The phospholipid content in camel milk is relatively high. Donkey milk contains metabolites that have potential therapeutic effects on mental disorders and chronic inflammatory diseases. Camel milk exhibits potential neuroprotective effects. Compared with other species, human milk contains more receptor protein-tyrosine kinase and galectin-3-binding protein; camel milk contains more monocyte differentiation antigen CD14 and fibrinogen beta chain; while pig milk contains more aminopeptidase. This research provides a theoretical basis for the application of featured milk in the field of functional foods and other food sectors.

## 1. Introduction

As nutritious beverages, dairy products are crucial for the growth of newborns. Especially, special milks such as donkey milk, mare milk and camel milk have attracted increasing attention and demand worldwide. These special kinds of milk not only have nutritional components similar to those of breast milk, but also perform excellently in terms of allergenicity and digestion, thus becoming good substitutes for cow milk (Li, Ma, Liu, & Wang, 2022; Mohamed, Johansson, Lundh, Nagy, & Kamal-Eldin, 2020). Although existing studies have revealed the differences in the nutritional components of milks from different animals (Hsu et al., 2021), there are still many unexplored areas in the omics data research on these special milks.

In recent years, significant progress has been made in the omics research of donkey milk, mare milk, and camel milk. Previous studies have analyzed CM adulteration in MM via proteomics and metabolomics. Statistical analyses showed that certain proteins in casein and secretoglobin family 1D member and metabolites like orotic acid and 4-aminonicotinic acid increased with higher CM percentage. These proteins and metabolites can distinguish MM adulterated with CM at 1 % level (Ji et al., 2023). Another study conducted quantitative analyses of whey proteins from texas donkeys with varying milk yields, identifying 216 whey proteins and determining those associated with milk yield traits (Zhang et al., 2019). Yanzhi wu and others conducted a non-targeted lipidomic analysis of 13 animal milk types, identifying 51 lipid subclasses and 2585 lipid molecules, discovering that the total lipid content in ruminants is higher than that in pseudo-ruminants and monogastric animals. They found that pig and camel milk contain higher levels of phospholipids, while donkey and mare milk components are closer to those of human milk. Pig milk was noted for its high content of long-chain polyunsaturated fatty acids, while ruminant milk exhibited characteristics of high short-chain fatty acids, with PS (22, 5_18,2) identified as a potential biomarker for pig milk, which has longer chain lengths and higher saturation levels, as well as higher ARA (arachidonic acid), DHA (docosahexaenoic acid), and EPA (eicosapentaenoic acid) contents compared to human milk (Wu et al., 2023). However, despite these research achievements, there remain many areas that require further exploration in the omics data studies of donkey, mare, and camel milk. For instance, the differences in omics data of milk from different breeds and under varied feeding conditions need to be investigated in

* Corresponding author.
*E-mail address:* wangzeying2012@syau.edu.cn (Z. Wang).
[1] These authors contributed equally to this work

https://doi.org/10.1016/j.fochx.2025.102592
Received 21 February 2025; Received in revised form 18 May 2025; Accepted 26 May 2025
Available online 27 May 2025

greater depth; the identification and elucidation of the mechanisms of action of certain potential metabolites with special functions also require further clarification.

As an emerging food resource, featured milk is rich in nutrition. However, due to its low yield, the research on its nutritional components and functional activities is relatively simple and its application technology is rather limited, which has led to the neglect of the nutritional value of the milk of some animals. The research on the nutritional composition and functional activities of featured milk is relatively single, and the application technology is rather limited. The nutritional functions of the animal milk of a few species have been neglected all the time due to the low economic benefits brought by the relatively low yield. To raise awareness of the significance of small animal milk products and to stimulate interest in their research and application, this study employed liquid chromatography-tandem mass spectrometry (LC-MS/MS) to accurately measure the absolute content of lipid molecules in specialty milk products. LC-MS/MS can accurately differentiate various types of lipid molecules and conduct specific detections, significantly enhancing measurement accuracy, and is also sensitive enough to detect low-abundance lipid molecules, thus providing robust support for a comprehensive understanding of the lipid composition of dairy products (Zhao et al., 2022). Ultra-high-performance liquid chromatography-quadrupole time-of-flight mass spectrometry (UHPLC-Q-TOF MS) was utilized to analyze highly differentially expressed metabolites in dairy products. UHPLC-Q-TOF MS boasts advantages such as high resolution, rapid analysis, and the provision of rich structural information and broad applicability, allowing for accurate analysis of highly differentially expressed metabolites in specialty milk products and providing comprehensive information for in-depth studies of their quality and functionality. Compared to traditional research methods, 4D label-free proteomics represents an advanced proteomics technology aimed at studying protein expression and function within biological systems. By comparing the lipid molecules, metabolites, and proteins in donkey milk, mare milk, and camel milk with those in human milk and pig milk, this study identified the significant differences that may affect the development of special dairy products. Integrating proteomics and metabolomics for multi-omics joint analysis, screening out key metabolites, and revealing the unique characteristics of these milk types. The research results provide valuable information for the development of specialized dairy products and a reference for the research and utilization of these milk sources. It also provides more systematic and comprehensive theoretical support for the improvement of the quality of featured milk and promotes the technological progress and sustainable development of the featured milk industry.

## 2. Materials and methods

### 2.1. Test sample collection

In the autumn of 2023, healthy mothers who tested negative for mastitis and other diseases were selected as experimental subjects. The specific situation is as follows: Chinese human milk samples (CHP) were generously donated by Chinese mothers from Shenyang Maternal and Child Health Care Center (All human milk samples were sourced from lactation centers of professional medical institutions and postpartum care centers, which have an abundant pool of lactating women). The Dongaijiao donkey breeding base in Fuxin Mongolian Autonomous County, Liaoning Province provided donkey milk samples from Fuxin, Liaoning (DZD). Mongolian mare milk samples (MGH) came from the Science and Technology Association of Xilingol League, Inner Mongolia. Alxa camel milk samples (ALC) were obtained from the Alxa Bactrian camel farm in Inner Mongolia. Pig milk samples (YXP) were provided by Yangxiang Pig Industry Group. For all the collected species, the number of samples for each variety is six. Milk samples were collected two weeks after the birth of the second litter. After each feeding or milking, the milk sample was extracted and placed in the same 10-ml plastic container. Then it was quickly refrigerated at −20 °C. The refrigeration time does not exceed two weeks. Subsequently, the samples were transported in undefrosted dry ice and stored in a freezer at −80 °C for long-term storage, but the storage time does not exceed four months.

**Ethical Statements**: Ethical approval for the involvement of human subjects in this study was granted by Shenyang Agricultural University Research Ethics Committee, Reference number 202106015.Human milk collection is conducted with the consent of the donors.Before the experiment began, we elaborated on the design and operation process of the experiment to the animal keepers and managers in detail to ensure that they understood and agreed to the conduct of the experiment. The data collected in this study may be used for further scientific research and, subject to compliance with laws and regulations, for the development of related commercial products or services.

### 2.2. Experimental instruments and reagents

The experimental instruments and reagents used in metabolomics, lipidomics, and proteomics are shown in appendix.

### 2.3. Milk sample processed

#### 2.3.1. Lipidomics

Lipids were extracted according to methyl-tert-butyl ether (MTBE) method. Take 150 μL of the milk sample and combine it with 200 μL of water and 20 μL of internal lipid standard mixture. Vortex the mixture vigorously. Then, add 800 μL of MTBE, and vortex again to mix thoroughly, followed by the addition of 240 μL of pre-cooled methanol. Vortex once more to ensure homogeneity. Subsequently, sonicate the solution in a low-temperature water bath for 20 min and allow it to stand at room temperature for 30 min. Centrifuge the mixture at 14000 ×*g* at 10 °C for 15 min and collect the upper organic phase. Dry it with nitrogen and add 200 μL of 90 % isopropanol/acetonitrile solution for reconstitution during mass spectrometry analysis. Vortex the reconstituted solution thoroughly and take 90 μL of it. Centrifuge at 14000 ×*g* at 10 °C for 15 min and collect the supernatant for injection analysis.

#### 2.3.2. Metabolomics

After the samples have been slowly thawed at 4 °C, take 150 μL of the milk sample and merge it with a pre-cooled solution of methanol/acetonitrile/water in a ratio of 2:2:1 (*v*/v). After intense vortexing and shaking, subject the mixture to low-temperature ultrasonication for 30 min, and subsequently let it settle at −20 °C for 10 min to facilitate precipitation. Centrifuge the solution at 14000 ×*g* at 4 °C for 20 min to remove impurities, and acquire the supernatant for mass spectrometry analysis. During the analysis process, add 100 μL of the acetonitrile-water solution with a ratio of acetonitrile: water being 1:1 (v/v) for re-suspension, vortex it thoroughly, and then centrifuge at 14000 ×*g* at 4 °C for 15 min before gathering the supernatant for subsequent analysis.

#### 2.3.3. Proteomics

*2.3.3.1. Protein extraction.* Milk samples were centrifuged at 1006.2 ×*g* for 15 min, the upper fat was discarded, and skim milk was collected. The skim milk was centrifuged at 1118000 ×*g* for 1 h (casein was removed), and the supernatant was collected as whey sample. Proteins were extracted by urea lysis buffer (UA) cleavage and quantified by bicinchoninic acid assay (BCA). Specifically, the appropriate amount of UA lysate was added, and the precipitate was resuspended by Votex, it was crushed by ultrasonic cell crusher, with the ultrasonic time of 30 s, the intermittent time of 30 s, and the working time of 40 min, and then it was centrifuged at 17468.75 ×*g* for 20 min at 21 °C, and the supernatant was taken and transferred to a new centrifuge tube. 20 μg protein from each sample was mixed with 5× loading buffer, boiled for 5 min, and

separated on 12.5 % SDS-PAGE gel (constant current 14 mA, 90 min). Coomassie brilliant blue R-250 staining showed protein bands.

*2.3.3.2. Enzymatic hydrolysis in solution.* Each sample, containing 200 μg of protein, was treated with 8 M UA for 1 h at room temperature. Dithiothreitol (DTT) was added to achieve a final concentration of 100 mM, and the mixture was shaken at 40.2 ×*g* for 1 min before being incubated at room temperature for an additional hour. Subsequently, IAA buffer (50 mM IAA in UA) was added and the solution was oscillated at 40.2 ×*g* for 1 min, followed by incubation at room temperature in the dark for 30 min. A 100 mM $NH_4HCO_3$ solution was added to dilute the 8 M UA to 2 M. Following this, 40 μL of Trypsin buffer (4 μg Trypsin in 40 μL 25 mM $NH_4HCO_3$) was added, and the solution was shaken at 40.2 ×*g* for 1 min and then incubated at 37 °C for 16–18 h. Trifluoroacetic acid (TFA) was used for acidification to adjust the pH to approximately 3. Subsequently, the peptides were desalted using MCX (Oasis ® MCX uElution Plate 30 um). After lyophilization, the peptides were redissolved in 40 μL of 0.1 % formic acid solution and then quantified at $OD_{280}$.

### 2.4. Chromatographic and mass spectrometry analysis

#### 2.4.1. Lipidomics

Reverse phase chromatography using a CSH C18 column (1.7 μm, 2.1 mm × 100 mm, Waters) was chosen for LC separation. The lipid extracts were re-dissolved in 200 μL of 90 % isopropanol/acetonitrile, centrifuged at 14000 ×*g* for 15 min, and finally, 3 μL of the sample was injected. Solvent A consisted of acetonitrile–water (6,4, *v*/v) with 0.1 % formic acid and 0.1 mM ammonium formate, while solvent B comprised acetonitrile–isopropanol (1,9, v/v) with 0.1 % formic acid and 0.1 mM ammonium formate. The initial mobile phase was 30 % solvent B at a flow rate of 300 μL/min. This composition was maintained for 2 min before linearly increasing to 100 % solvent B over 23 min, followed by equilibration at 5 % solvent B for 10 min. Mass spectra were acquired by Q-Exactive Plus in positive and negative modes, respectively. The ESI parameters were optimized and preset for all measurements as follows: Source temperature, 300 °C; Capillary Temp, 350 °C; the ion spray voltage was set at 3000 V; S-Lens RF Level was set at 50 %; and the scan range of the instruments was set at *m/z* 200–1800 (Damen, Isaac, Langridge, et al., 2014).

#### 2.4.2. Metabolomics

*2.4.2.1. Chromatography-mass spectrometry.* This study employs high-resolution untargeted metabolomics, which involves matching metabolite retention times in local databases, molecular mass (with an error within <10 ppm), secondary fragmentation spectra, collision energies, and other relevant parameters of metabolites present in biological samples. The metabolites in the biological samples are structurally identified and the results are rigorously checked and confirmed manually (Zhang et al., 2019).

*2.4.2.2. Chromatographic conditions.* The samples underwent separation using the Agilent 1290 Infinity LC ULTRA high Performance Liquid Chromatography (UHPLC) HILIC column. The column temperature was set at 25 °C, with a flow rate of 0.5 mL/min and an injection volume of 2 μL. The mobile phase composition was as follows: A (water +25 mM ammonium acetate +25 mM ammonia water) and B (acetonitrile). The gradient elution procedure proceeded as follows: 0–0.5 min, 95 % B; 0.5–7 min, B linearly decreased from 95 % to 65 %; 7–8 min, B linearly decreased from 65 % to 40 %; 8–9 min, B remained at 40 %; 9–9.1 min, B linearly increased from 40 % to 95 %; 9.1–12 min, B maintained at 95 %. Throughout the analysis, the samples were stored in an automatic sampler at 4 °C to minimize the impact of signal fluctuations from instrument detection. A random sequence was employed for the continuous analysis of samples to mitigate the influence of instrument detection signal fluctuation. Quality control (QC) samples were interspersed within the sample queue to monitor and assess the stability of the system and the reliability of experimental data.

*2.4.2.3. Q-TOF mass spectrometry conditions.* The samples underwent separation using the Agilent 1290 Infinity LC ULTRA high performance liquid chromatography (UHPLC) system and were analyzed by the AB Sciex Triple TOF 6600 mass spectrometer. Electrospray ionization (ESI) was utilized in both positive and negative ion modes for detection. The ESI source parameters were set as follows: atomizing gas auxiliary heating 1 (Gas1): 60, auxiliary heating 2 (Gas2): 60, air curtain gas (CUR): 30 PSI, ion source temperature: 600 °C, and spray voltage (ISVF) ±5500 V (positive and negative modes).

The primary mass charge ratio detection range was 60–1000 Da, while the secondary ion mass charge ratio detection range was 25–1000 Da. The primary mass spectrometry scanning cumulative time was 0.20 s/spectrum, and the secondary mass spectrometry scanning cumulative time was 0.05 s/spectrum. The secondary mass spectrometry was acquired using data-dependent acquisition mode (IDA) and peak intensity value screening mode. The cluster removal voltage (DP) was set at ±60 V (positive and negative modes), and the collision energy was 35 ± 15 eV.

The IDA parameters included a dynamic exclusion isotope ion range of 4 Da, with 10 fragment profiles collected in each scan(Nie et al., 2019).

#### 2.4.3. Proteomics

The separation was performed using the nano-flow HPLC system Easy nLC. The buffer consisted of 0.1 % formic acid aqueous solution for Solution A, and 0.1 % formic acid acetonitrile aqueous solution (84 % acetonitrile) for Solution B. The chromatographic column was equilibrated with 95 % Solution A. The sample was loaded onto a Thermo Scientific EASY column (2 cm*100 μm 5 μm-C18) and separated on a Thermo Scientific EASY column (75 μm*100 mm 3 μm-C18) at a flow rate of 300 nL/min. The liquid phase gradient was as follows: a 1-h gradient with B liquid linearly transitioning from 0 % to 35 % from 0 min to 50 min, then from 35 % to 100 % from 50 min to 55 min, and maintained at 100 % from 55 min to 60 min. The peptides were separated by chromatography and analyzed by the timsTOF Pro mass spectrometer. The machine's MS detection time was 60 min, operating in positive ion mode. The MS scan range was set to 100–1700 *m/z*. The data acquisition mode was parallel accumulation serial fragmentation (PASEF) mode. Following the first-order MS acquisition, the parent ion was collected in 10 PASEF mode, with a period window time of 1.17 s (Suo, Liang, Zhang, et al., 2024).

### 2.5. Data analysis

#### 2.5.1. Lipidomics data analysis

"Lipid Search" is a search engine designed for the identification of lipid species using MS/MS analysis. Lipid Search encompasses over 30 lipid classes and more than 1,500,000 fragment ions in its database. The mass tolerance for both precursor and fragment was set to 5 ppm. Lipid species were identified using the LipidSearch software version 4.2 (Thermo Scientific™) to process the raw data and for peak alignment, retention time correction and extraction peak area. Adducts of +H, $+NH_4$ were selected for positive mode searches, and —H, $+CH_3COO$ were selected for negative mode searches since ammonium acetate was used in the mobile phases. For the data extracted from LipidSearch, remove the ion peak with a value of >50 % missing from the group.

#### 2.5.2. Metabolomics data analysis

The original data in Wiff format is converted to ".mzXML" format by ProteoWizard, and then peak alignment, retention time correction, and

peak area extraction are performed using XCMS software. The data extracted by XCMS is first subjected to metabolite structure identification, data preprocessing, experimental data quality evaluation, and finally data analysis. The data analysis content includes differential metabolite screening, cluster analysis, and correlation analysis of differential metabolites.

#### 2.5.3. Proteomic data analysis

The original data of mass spectrometry analysis were .D files, and Peaks software was used for database identification and quantitative analysis. The database used is Uniprot. *Homo sapiens* (Human) [9606], Equus [9789], *Camelus dromedarius* (Dromedary) (Arabian camel) [9838], *Sus scrofa* (Pig) [9823]. Use CELLO software for subcellular localization analysis of all expressed proteins. Search protein sequences using InterPro Scan software and predict the protein domain structures through InterPro Scan software. Utilize Blast2GO software for gene ontology (GO) term localization and sequence annotation. GO annotation results are plotted using R script. Perform Kyoto Encyclopedia of Genes and Genomes (KEGG) pathway annotation on the target protein set using KAAS (KEGG Automatic Annotation Server) software.

#### 2.5.4. Multi - omics integration data analysis

With the help of KEGG pathway integration analysis, compared the pathways in which proteins and metabolites with differential expression in the proteome are involved, and obtain the metabolic pathways and their quantities that are commonly involved in both omics. Using R software and Cytoscape software to draw matrix heat maps, hierarchical clustering heat maps, and correlation network graphs, and then conducting correlation analysis to explore the interaction relationships between substances from multiple perspectives.

## 3. Results

### 3.1. Lipidomics

#### 3.1.1. Total lipid content

The total lipid content of a species is calculated by summing the quantified amounts of all lipid molecules within that species. It represents the overall content of lipid molecules in the species. As illustrated in Fig. 1A, ALC has the highest total lipid content, MGH has the lowest total lipid content.

#### 3.1.2. Composition of lipid subclasses

The composition of lipid subclasses in different animals is presented in a circular diagram. As illustrated in Fig. 1B, TG are the most abundant lipid in five species, followed by PE, PC, SM, PS, Cer, and PI.

#### 3.1.3. Lipid class levels

Different lipid subclasses have distinct biological functions. Changes in the abundance of lipid subclasses can reflect alterations in lipid functionality. As illustrated in Fig. 1C, in both Pos and Neg ion modes, a total of 2585 lipid species belonging to 51 different lipid categories were detected. Among these lipids, a subset of 13 lipid categories showed over 50 annotations. These lipid categories include ceramides (Cer), cardiolipins (CL), diacylglycerols (DG), monohexosylceramides (Hex1Cer), dihexosylceramides (Hex2Cer), phosphatidic acids (PA), phosphatidylcholines (PC), phosphatidylethanolamines (PE), phosphatidylglycerols (PG), phosphatidylinositols (PI), phosphatidylserines (PS), sphingomyelins (SM), and triglycerides (TG).

#### 3.1.4. Screening differential lipid molecules

The variable importance in projection (VIP) values obtained from the orthogonal projection to latent structures - discriminant analysis (OPLS-DA) model can be used to assess the impact strength and explanatory power of the expression patterns of lipid molecules on sample classification discrimination. It helps in identifying differentially expressed lipid molecules with biological significance. Typically, lipid molecules with VIP $>$ 1 are considered to have a significant contribution to the model interpretation. In this experiment, the criteria for selecting significant differential lipid molecules are OPLS-DA VIP $>$ 1 and $P$ value $<$0.05. Using these criteria, a total of 59 differential lipid molecules were selected, including the top 20 highly abundant lipid molecules in both the Pos and Neg ion modes, as well as some lipid molecules with important functionalities. These 59 lipid molecules are collectively referred to as differential lipid molecules.

As shown in Table 1, based on the criteria of differential lipid molecule abundance, compared with CHP and YXP, in the Pos mode, DZD does not have any significant differential lipid molecules. MGH has 12 significant differential lipid molecules, including 8 TGs, 2 DGs, and 2 AcylGlcCholesterol ester (AcHexchEs). ALC has 4 significant differential lipid molecules, including 2 PEs, 1 PC, and 1 Bis-methyl phosphatidic acid (BisMePA). In the Neg mode, both DZD and MGH do not have any significant differential lipid molecules. ALC has 12 significant differential lipid molecules, including 3 PEs, 2 PCs, 3 PIs, 2 Cers, 1 CL, and 1 Hex1Cer.

#### 3.1.5. Cluster Heatmap

To assess the rationality of differential lipid molecules and to provide a more comprehensive and intuitive display of the relationships between species, as well as the expression pattern differences of lipid molecules across different species. Perform heatmap analysis on differential lipid molecules. As illustrated in Fig. 1D, the clustering results indicate that DZD and MGH exhibit similar expression trends for differential lipid molecules. The expression of lipid molecules within the species CHP, DZD, MGH, ALC, and YXP demonstrates interspecies differences.

### 3.2. Metabolomics

#### 3.2.1. Chemical classification

To classify and analyze all metabolites identified in CHP, DZD, MGH, ALC, and YXP, we can perform a statistical analysis based on their chemical classification attribution information. As illustrated in Fig. 2A, among CHP, DZD, MGH, ALC, and YXP, the largest proportion of metabolites belongs to the category “Lipids and lipid-like molecules,” accounting for 5.203 %. On the other hand, the smallest proportion of metabolites belongs to the category “Organophosphorus compounds” representing only 0.02 %.

#### 3.2.2. Metabolite screening

Metabolomics studies often employ strict criteria such as VIP $>$ 1 and $P$-value $<$0.05 to identify significantly different metabolites. Using these criteria as screening standards, we can select the top 20 differentially expressed metabolites in CHP, DZD, MGH, ALC, and YXP under both the Pos and Neg ion modes, as well as metabolites with important functions. As illustrated in Table 2, based on the comparison of differential metabolite levels between CHP and YXP, the expression of differential metabolites in DZD, MGH, and ALC shows significant interspecies variation. Under the Pos mode: DZD has 1 significant differential metabolite: xanthurenic acid. MGH has 3 significant differential metabolites: acridinone, ethylmorphine, and gabapentin. ALC has 6 significant differential metabolites: 1,1,3-trimethylurea, barbamate, dodemorph, ethosuximide, l-deprenyl, and niacinamide. Neg mode, DZD has 1 significant differential metabolite: 1-stearoyl-2-hydroxy-sn-glycero-3-phosphate. MGH has 7 significant differential metabolites: tenofovir, daidzein, 4.alpha.-mannobiose, isopentenyl pyrophosphate, erythritol, l-threonine, and l-valine. ALC has 1 significant differential metabolite: allantoin.

#### 3.2.3. Differential metabolite bioinformatics analysis

*3.2.3.1. Cluster analysis.* The purpose of differential metabolite

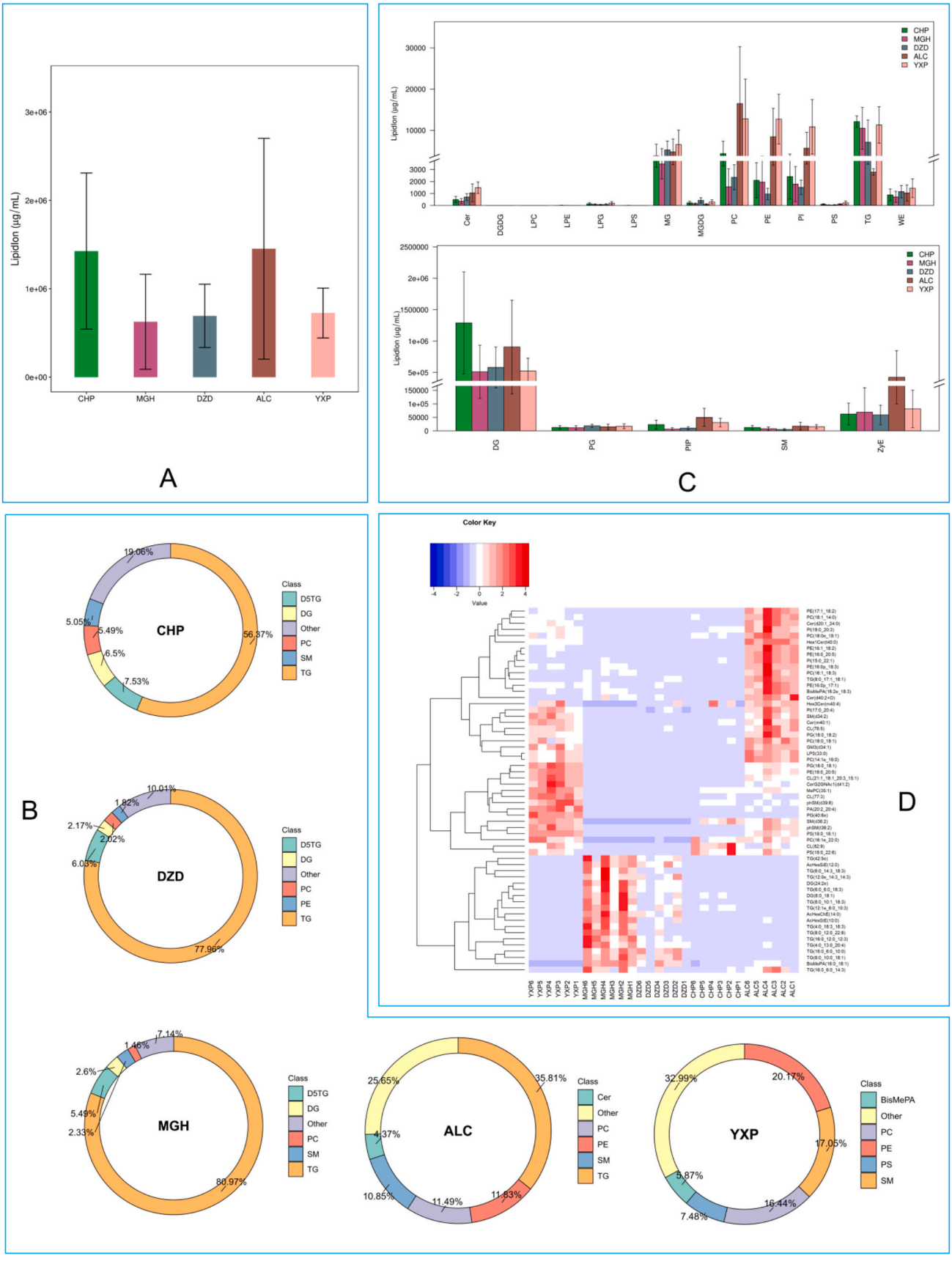


**Fig. 1.** (A) Total lipid content; (B) Lipid subclass composition; (C) Statistics of lipid subclass content; (D) Heat map of clustering of differential lipid molecules.

**Table 1**
Differential lipid molecules.

| LipidIon(ug/mL) | CHP | DZD | MGH | ALC | YXP |
|---|---|---|---|---|---|
| Cer(d20:1_24:0) | 0.09 ± 0.04 | 0.02 ± 0.01 | 0.03 ± 0.01 | 1.42 ± 0.65 | 0.43 ± 0.18 |
| SM(d34:2) | 0.37 ± 0.17 | 0.01 ± 0.01 | 0.02 ± 0.01 | 2.54 ± 1.51 | 2.67 ± 1.16 |
| phSM(t36:2) | 0.23 ± 0.17 | 0.01 ± 0.00 | 0.01 ± 0.01 | 1.48 ± 0.56 | 2.32 ± 0.72 |
| Cer(m40:1) | 0.12 ± 0.07 | 0.02 ± 0.01 | 0.01 ± 0.01 | 0.45 ± 0.28 | 0.37 ± 0.15 |
| PG(18:0_18:2) | 0.04 ± 0.02 | 0.05 ± 0.03 | 0.02 ± 0.01 | 0.96 ± 0.61 | 0.44 ± 0.14 |
| PG(18:0_18:1) | 0.03 ± 0.01 | 0.01 ± 0.00 | 0.02 ± 0.01 | 0.11 ± 0.07 | 0.34 ± 0.09 |
| GM3(d34:1) | 0.03 ± 0.01 | 0.01 ± 0.00 | 0.01 ± 0.00 | 0.60 ± 0.12 | 0.50 ± 0.28 |
| Hex1Cer(t40:0) | 0.93 ± 0.30 | 0.35 ± 0.21 | 0.21 ± 0.10 | 17.68 ± 5.06 | 3.48 ± 0.92 |
| PE(16:1_18:2) | 0.02 ± 0.01 | 0.31 ± 0.17 | 0.40 ± 0.26 | 9.12 ± 3.85 | 0.96 ± 0.64 |
| CL(82:9) | 0.92 ± 0.57 | 0.01 ± 0.00 | 0.01 ± 0.00 | 0.30 ± 0.14 | 0.61 ± 0.37 |
| PG(40:6e) | 0.01 ± 0.00 | 0.02 ± 0.00 | 0.03 ± 0.01 | 0.01 ± 0.00 | 0.67 ± 0.14 |
| SM(d36:2) | 0.84 ± 0.45 | 0.01 ± 0.00 | 0.01 ± 0.01 | 0.92 ± 0.38 | 1.33 ± 0.21 |
| PA(20:2_20:4) | 0.05 ± 0.03 | 0.03 ± 0.01 | 0.03 ± 0.01 | 0.20 ± 0.09 | 3.02 ± 0.89 |
| PE(17:1_18:2) | 0.02 ± 0.01 | 0.13 ± 0.10 | 0.09 ± 0.04 | 4.91 ± 1.92 | 0.57 ± 0.27 |
| LPS(33:0) | 0.10 ± 0.04 | 0.07 ± 0.05 | 0.11 ± 0.03 | 2.13 ± 0.50 | 1.28 ± 0.50 |
| CerG2GNAc1(d41:2) | 0.01 ± 0.00 | 0.01 ± 0.00 | 0.02 ± 0.02 | 0.16 ± 0.05 | 1.22 ± 0.60 |
| PS(18:0_22:6) | 3.88 ± 3.08 | 0.01 ± 0.01 | 0.02 ± 0.02 | 2.76 ± 1.70 | 2.63 ± 1.51 |
| PC(14:1e_16:0) | 0.10 ± 0.04 | 0.07 ± 0.06 | 0.11 ± 0.03 | 2.17 ± 0.50 | 1.32 ± 0.50 |
| CL(21:1_18:1_20:3_15:1) | 0.11 ± 0.06 | 0.03 ± 0.01 | 0.03 ± 0.01 | 0.55 ± 0.21 | 1.40 ± 0.46 |
| PC(18:0e_18:1) | 0.47 ± 0.16 | 0.04 ± 0.04 | 0.07 ± 0.02 | 1.94 ± 0.52 | 0.70 ± 0.27 |
| PE(18:0_20:5) | 0.39 ± 0.26 | 0.13 ± 0.07 | 0.06 ± 0.04 | 3.52 ± 1.41 | 7.65 ± 1.85 |
| PC(16:1e_22:0) | 1.07 ± 0.53 | 0.05 ± 0.05 | 0.05 ± 0.02 | 1.11 ± 0.41 | 1.60 ± 0.70 |
| PE(16:0_20:5) | 0.01 ± 0.00 | 0.00 ± 0.00 | 0.02 ± 0.01 | 1.03 ± 0.43 | 0.08 ± 0.06 |
| AcHexSiE(12:0) | 0.11 ± 0.08 | 1.52 ± 1.16 | 3.22 ± 1.25 | 0.17 ± 0.10 | 0.00 ± 0.00 |
| MePC(35:1) | 1.36 ± 0.75 | 0.07 ± 0.07 | 0.01 ± 0.01 | 1.77 ± 0.62 | 4.90 ± 1.39 |
| TG(4:0_13:0_20:4) | 0.01 ± 0.01 | 0.11 ± 0.06 | 0.75 ± 0.43 | 0.06 ± 0.03 | 0.00 ± 0.00 |
| TG(8:0_17:1_18:1) | 0.01 ± 0.02 | 0.08 ± 0.09 | 0.08 ± 0.05 | 1.11 ± 0.46 | 0.01 ± 0.00 |
| PC(18:1_14:0) | 0.07 ± 0.06 | 0.02 ± 0.01 | 0.01 ± 0.01 | 0.82 ± 0.31 | 0.17 ± 0.05 |
| PE(16:0p_18:3) | 0.09 ± 0.05 | 0.13 ± 0.11 | 0.73 ± 0.33 | 5.24 ± 2.50 | 0.74 ± 0.36 |
| TG(8:0_10:1_18:3) | 0.04 ± 0.04 | 2.33 ± 2.66 | 19.02 ± 11.75 | 0.20 ± 0.06 | 0.01 ± 0.00 |
| PS(18:0_18:1) | 0.20 ± 0.15 | 0.07 ± 0.07 | 0.07 ± 0.05 | 2.10 ± 0.64 | 3.68 ± 0.37 |
| PI(18:0_20:3) | 4.64 ± 2.40 | 0.50 ± 0.38 | 0.84 ± 0.48 | 20.1 ± 10.9 | 7.21 ± 2.62 |
| DG(24:2e) | 0.01 ± 0.00 | 0.12 ± 0.09 | 0.85 ± 0.53 | 0.02 ± 0.01 | 0.03 ± 0.01 |
| TG(42:5e) | 0.01 ± 0.00 | 0.25 ± 0.22 | 1.08 ± 0.73 | 0.01 ± 0.01 | 0.01 ± 0.00 |
| AcHexChE(14:0) | 0.12 ± 0.07 | 0.92 ± 0.88 | 3.02 ± 1.42 | 0.14 ± 0.11 | 0.03 ± 0.02 |
| TG(8:0_12:0_22:6) | 0.01 ± 0.01 | 0.09 ± 0.09 | 1.05 ± 0.41 | 0.04 ± 0.02 | 0.01 ± 0.00 |
| AcHexSiE(10:0) | 0.04 ± 0.03 | 0.17 ± 0.09 | 0.98 ± 0.32 | 0.12 ± 0.03 | 0.01 ± 0.00 |
| PE(16:0p_17:1) | 0.01 ± 0.00 | 0.06 ± 0.04 | 0.08 ± 0.04 | 0.51 ± 0.22 | 0.12 ± 0.03 |
| TG(16:0_6:0_10:0) | 0.47 ± 0.57 | 9.20 ± 6.16 | 12.00 ± 4.46 | 0.32 ± 0.14 | 0.06 ± 0.04 |
| TG(4:0_18:3_18:3) | 0.03 ± 0.02 | 0.40 ± 0.30 | 14.62 ± 10.62 | 0.16 ± 0.10 | 0.01 ± 0.01 |
| TG(6:0_14:3_18:3) | 0.00 ± 0.00 | 0.05 ± 0.05 | 1.39 ± 1.21 | 0.03 ± 0.02 | 0.02 ± 0.00 |
| DG(8:0_18:1) | 0.54 ± 0.50 | 0.72 ± 0.73 | 3.77 ± 2.23 | 0.03 ± 0.01 | 0.00 ± 0.00 |
| BisMePA(16:2e_18:3) | 0.12 ± 0.06 | 0.13 ± 0.16 | 0.94 ± 0.51 | 7.40 ± 3.11 | 0.60 ± 0.40 |
| TG(12:1e_6:0_10:3) | 0.45 ± 0.38 | 0.66 ± 0.67 | 3.10 ± 2.02 | 0.01 ± 0.00 | 0.00 ± 0.00 |
| BisMePA(16:0_18:1) | 0.16 ± 0.15 | 1.78 ± 1.13 | 3.61 ± 0.56 | 0.90 ± 0.26 | 0.01 ± 0.01 |
| PI(17:0_20:4) | 0.03 ± 0.01 | 0.02 ± 0.03 | 0.04 ± 0.02 | 0.27 ± 0.13 | 0.22 ± 0.09 |
| TG(16:0_12:0_12:3) | 0.02 ± 0.01 | 0.08 ± 0.06 | 0.42 ± 0.24 | 0.02 ± 0.01 | 0.02 ± 0.01 |
| PC(18:0_18:1) | 0.99 ± 0.99 | 0.07 ± 0.05 | 0.05 ± 0.05 | 6.4 ± 1.86 | 3.26 ± 2.28 |
| TG(12:0e_14:3_14:3) | 0.01 ± 0.01 | 0.21 ± 0.26 | 0.48 ± 0.47 | 0.01 ± 0.01 | 0.01 ± 0.00 |
| TG(6:0_6:0_18:3) | 0.06 ± 0.06 | 0.33 ± 0.31 | 4.12 ± 3.25 | 0.02 ± 0.01 | 0.01 ± 0.00 |
| CL(78:5) | 0.02 ± 0.02 | 0.03 ± 0.02 | 0.01 ± 0.01 | 0.23 ± 0.11 | 0.14 ± 0.04 |
| CL(77:3) | 0.16 ± 0.17 | 0.03 ± 0.04 | 0.04 ± 0.02 | 0.30 ± 0.09 | 3.77 ± 1.24 |
| TG(6:0_10:0_18:1) | 10.52 ± 15.96 | 183.39 ± 163.33 | 366.82 ± 169.27 | 24.74 ± 18.19 | 1.19 ± 0.53 |
| Hex3Cer(m40:4) | 0.04 ± 0.04 | 0.03 ± 0.02 | 0.00 ± 0.00 | 0.07 ± 0.01 | 0.05 ± 0.04 |
| phSM(d39:8) | 0.11 ± 0.07 | 0.01 ± 0.01 | 0.01 ± 0.01 | 0.08 ± 0.02 | 0.47 ± 0.16 |
| PI(15:0_22:1) | 0.00 ± 0.00 | 0.00 ± 0.00 | 0.01 ± 0.01 | 0.15 ± 0.06 | 0.01 ± 0.01 |
| Cer(d40:2 O) | 0.01 ± 0.01 | 0.01 ± 0.01 | 0.03 ± 0.02 | 0.12 ± 0.05 | 0.01 ± 0.00 |
| PC(16:1_18:3) | 0.05 ± 0.05 | 0.05 ± 0.07 | 0.33 ± 0.19 | 1.56 ± 0.90 | 0.03 ± 0.03 |
| TG(16:0_6:0_14:3) | 0.03 ± 0.02 | 0.06 ± 0.05 | 0.23 ± 0.16 | 0.21 ± 0.14 | 0.01 ± 0.00 |

correlation analysis is to investigate the consistency of the variation trends among metabolites and discover the changing characteristics of metabolites across different samples. Performing a cluster heatmap analysis of the filtered differentially expressed metabolites. As illustrated in Fig. 2B, the clustering results reveal the variation trend of differential metabolites within different species exhibits interspecific variability.

*3.2.3.2. Correlation analysis.* Relatedness analysis can help measure the metabolic closeness between metabolites. As illustrated in Fig. 2C, in Pos mode, 4-amino-9-methoxypsoralen, 2,6-dihydroxy-4-methylbenzoic acid, 3-methyladenine, and valeroyl salicylate exhibit strong relatedness with other metabolites. In the Neg mode, 3′-sialyllactose shows strong relatedness with other metabolites.

### 3.3. Proteomics

#### 3.3.1. Quantitative analysis of proteins

Quantitative analysis of the identified proteins from all samples was performed using 4D-label-Free and Graphad Prism software. As shown in Fig. 3A, the highest number of proteins was detected in CHP, with a total of 1149 proteins. YXP, on the other hand, had the lowest number of proteins, with only 442 commonly identified proteins.

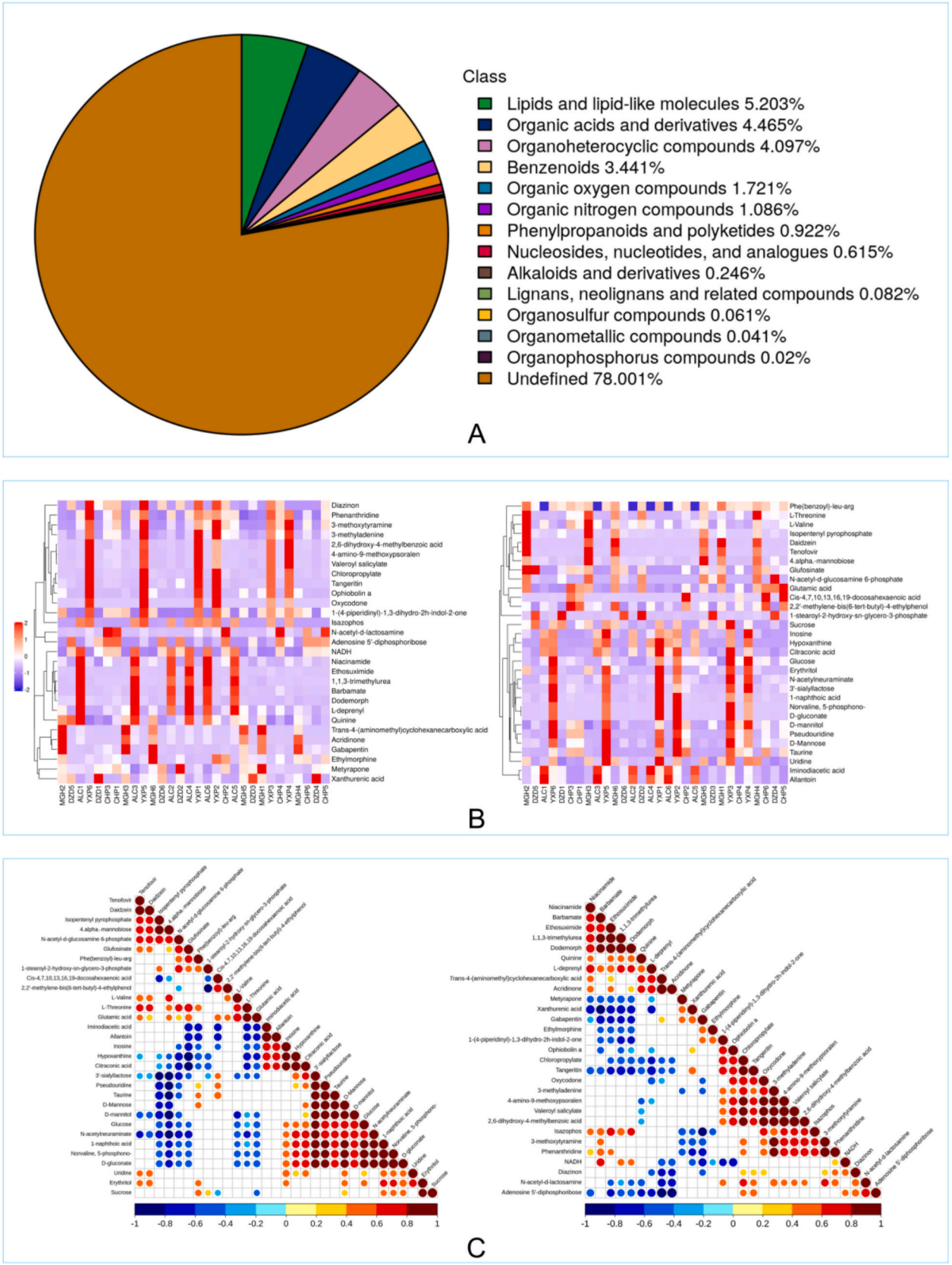


**Fig. 2.** (A) Statistical chart of chemical classifications; (B) Heat map of differential metabolite clustering; (C) Differential metabolite correlation analysis.

**Table 2**
Discrepant metabolites.

| Name | CHP | MGH | DZD | ALC | YXP |
|---|---|---|---|---|---|
| 1,1,3-trimethylurea | 2.70E+06 ± 1.06E+05 | 2.34E+06 ± 4.40E+05 | 2.42E+06 ± 2.42E+06 | 2.03E+07 ± 1.99E+06 | 2.53E+06 ± 1.86E+05 |
| NADH | 7.87E+07 ± 8.56E+06 | 1.80E+05 ± 1.48E+05 | 6.79E+07 ± 6.79E+07 | 1.36E+08 ± 8.33E+06 | 4.68E+06 ± 1.18E+06 |
| *N*-acetyl-d-lactosamine | 2.88E+09 ± 5.39E+08 | 1.05E+07 ± 4.91E+06 | 4.99E+07 ± 4.99E+07 | 1.55E+07 ± 5.34E+06 | 3.36E+08 ± 9.45E+07 |
| Adenosine 5′-diphosphoribose | 7.87E+07 ± 8.56E+06 | 8.37E+05 ± 3.92E+05 | 6.79E+07 ± 6.79E+07 | 7.05E+05 ± 1.30E+05 | 1.81E+07 ± 7.10E+06 |
| Isazophos | 7.96E+05 ± 2.22E+05 | 7.79E+05 ± 3.96E+05 | 2.17E+06 ± 2.17E+06 | 1.36E+08 ± 8.33E+06 | 1.49E+08 ± 2.02E+07 |
| L-deprenyl | 4.17E+07 ± 1.43E+07 | 6.80E+07 ± 1.22E+07 | 2.65E+06 ± 2.65E+06 | 2.46E+08 ± 2.76E+07 | 2.97E+06 ± 9.99E+05 |
| Trans-4-(aminomethyl)cyclohexanecarboxylic acid | 1.54E+07 ± 9.76E+06 | 4.04E+09 ± 1.67E+09 | 7.29E+06 ± 7.29E+06 | 4.44E+08 ± 2.92E+07 | 1.35E+07 ± 3.45E+06 |
| 1-(4-piperidinyl)-1,3-dihydro-2 h-indol-2-one | 7.87E+07 ± 8.56E+06 | 9.24E+07 ± 1.48E+07 | 1.30E+06 ± 1.30E+06 | 5.73E+05 ± 3.14E+05 | 1.49E+08 ± 2.02E+07 |
| Acridinone | 2.53E+06 ± 1.71E+06 | 9.41E+08 ± 4.59E+08 | 1.12E+06 ± 1.12E+06 | 1.07E+08 ± 9.45E+06 | 2.75E+06 ± 1.05E+06 |
| 4-amino-9-methoxypsoralen | 7.34E+06 ± 1.80E+06 | 4.32E+06 ± 8.72E+05 | 3.09E+06 ± 3.09E+06 | 5.29E+06 ± 3.71E+05 | 7.82E+07 ± 2.04E+07 |
| Dodemorph | 7.76E+06 ± 1.73E+06 | 7.90E+06 ± 1.44E+06 | 8.25E+06 ± 8.25E+06 | 4.85E+07 ± 4.25E+06 | 8.94E+06 ± 1.02E+06 |
| 3-methyladenine | 2.13E+07 ± 3.38E+06 | 6.75E+06 ± 2.40E+06 | 4.36E+06 ± 4.36E+06 | 1.40E+07 ± 2.55E+06 | 6.39E+07 ± 9.95E+06 |
| 3-methoxytyramine | 3.99E+07 ± 8.02E+06 | 3.61E+06 ± 1.30E+06 | 3.52E+06 ± 3.52E+06 | 2.68E+07 ± 6.05E+06 | 8.12E+07 ± 1.44E+07 |
| Xanthurenic acid | 1.13E+06 ± 4.51E+05 | 1.44E+07 ± 3.57E+06 | 3.39E+07 ± 3.39E+07 | 2.60E+05 ± 1.91E+05 | 6.47E+06 ± 2.24E+06 |
| Ethosuximide | 4.65E+06 ± 1.86E+06 | 7.72E+06 ± 3.91E+06 | 4.94E+06 ± 4.94E+06 | 4.88E+08 ± 6.71E+07 | 1.40E+07 ± 8.07E+06 |
| Chloropropylate | 7.37E+06 ± 2.68E+06 | 2.53E+06 ± 2.13E+06 | 1.87E+06 ± 1.87E+06 | 4.11E+05 ± 2.97E+05 | 1.49E+08 ± 2.02E+07 |
| Valeroyl salicylate | 3.59E+07 ± 8.98E+06 | 1.97E+07 ± 5.04E+06 | 1.33E+07 ± 1.33E+07 | 2.58E+07 ± 2.00E+06 | 4.22E+08 ± 1.15E+08 |
| Ophiobolin a | 1.11E+06 ± 2.95E+05 | 2.96E+07 ± 1.04E+07 | 1.75E+06 ± 1.75E+06 | 1.11E+06 ± 5.80E+05 | 1.49E+08 ± 2.02E+07 |
| Tangeritin | 6.08E+06 ± 2.61E+06 | 5.31E+06 ± 4.79E+06 | 9.98E+06 ± 9.98E+06 | 1.28E+05 ± 4.87E+04 | 1.49E+08 ± 2.02E+07 |
| 2,6-dihydroxy-4-methylbenzoic acid | 1.07E+07 ± 3.30E+06 | 6.74E+06 ± 1.47E+06 | 4.22E+06 ± 4.22E+06 | 8.11E+06 ± 9.54E+05 | 1.34E+08 ± 3.58E+07 |
| Oxycodone | 8.51E+04 ± 4.48E+04 | 8.38E+04 ± 4.18E+04 | 3.42E+05 ± 3.42E+05 | 1.99E+05 ± 1.39E+05 | 6.30E+07 ± 2.54E+07 |
| Gabapentin | 1.68E+07 ± 9.63E+06 | 2.20E+08 ± 8.39E+07 | 1.22E+07 ± 1.22E+07 | 9.68E+05 ± 8.00E+05 | 2.55E+06 ± 1.03E+06 |
| Phenanthridine | 1.12E+07 ± 2.58E+06 | 2.85E+06 ± 1.04E+06 | 2.91E+06 ± 2.91E+06 | 1.23E+07 ± 1.34E+06 | 1.92E+07 ± 2.07E+06 |
| Barbamate | 6.44E+06 ± 5.46E+06 | 1.88E+05 ± 1.10E+05 | 7.80E+05 ± 7.80E+05 | 1.36E+08 ± 8.33E+06 | 1.54E+06 ± 7.30E+05 |
| Niacinamide | 6.83E+08 ± 2.68E+08 | 6.42E+08 ± 1.43E+08 | 2.80E+08 ± 2.80E+08 | 3.05E+09 ± 2.59E+08 | 5.80E+08 ± 1.71E+08 |
| Quinine | 1.15E+07 ± 3.15E+06 | 2.40E+07 ± 5.03E+06 | 1.43E+07 ± 1.43E+07 | 3.13E+07 ± 1.29E+07 | 1.01E+07 ± 5.62E+06 |
| Diazinon | 6.68E+07 ± 3.36E+07 | 4.57E+05 ± 2.17E+05 | 5.61E+07 ± 5.61E+07 | 5.62E+06 ± 2.21E+06 | 1.28E+08 ± 6.47E+07 |
| Metyrapone | 4.30E+06 ± 8.92E+05 | 4.93E+06 ± 1.88E+06 | 6.03E+06 ± 6.03E+06 | 2.70E+06 ± 6.08E+05 | 3.39E+06 ± 2.13E+05 |
| Ethylmorphine | 2.15E+06 ± 1.09E+06 | 3.47E+06 ± 4.50E+06 | 6.33E+05 ± 6.33E+05 | 2.71E+05 ± 9.82E+04 | 1.28E+06 ± 1.93E+06 |
| Phe(benzoyl)-leu-arg | 2.07E+08 ± 1.27E+07 | 2.51E+08 ± 3.40E+07 | 1.75E+08 ± 1.84E+07 | 2.76E+05 ± 1.58E+05 | 2.00E+08 ± 1.72E+07 |
| Hypoxanthine | 2.50E+07 ± 1.38E+07 | 1.77E+07 ± 1.03E+07 | 1.31E+07 ± 7.76E+06 | 6.98E+09 ± 8.62E+08 | 8.52E+09 ± 1.94E+09 |
| Tenofovir | 1.85E+06 ± 4.66E+05 | 2.69E+08 ± 7.82E+07 | 1.58E+06 ± 5.80E+05 | 1.55E+06 ± 7.77E+05 | 2.00E+06 ± 3.40E+05 |
| Norvaline, 5-phosphono- | 5.36E+06 ± 2.56E+06 | 2.34E+06 ± 7.88E+05 | 2.31E+06 ± 1.31E+06 | 3.22E+06 ± 1.17E+06 | 3.78E+08 ± 1.21E+08 |
| *N*-acetyl-d-glucosamine 6-phosphate | 9.32E+06 ± 5.20E+06 | 3.34E+09 ± 3.16E+08 | 2.06E+09 ± 2.21E+09 | 2.34E+06 ± 1.76E+06 | 5.33E+06 ± 2.63E+06 |
| Pseudouridine | 3.06E+07 ± 1.21E+07 | 3.97E+06 ± 1.62E+06 | 4.11E+06 ± 1.16E+06 | 4.01E+06 ± 9.11E+05 | 7.85E+07 ± 1.30E+07 |
| 3′-sialyllactose | 8.99E+07 ± 3.53E+07 | 2.58E+06 ± 9.64E+05 | 2.94E+06 ± 2.90E+06 | 9.91E+06 ± 1.29E+06 | 9.50E+08 ± 2.89E+08 |
| Cis-4,7,10,13,16,19-docosahexaenoic acid | 3.94E+09 ± 2.09E+09 | 1.68E+07 ± 1.35E+07 | 8.23E+05 ± 4.06E+05 | 4.34E+06 ± 4.95E+05 | 1.27E+07 ± 8.50E+06 |

(*continued on next page*)

**Table 2** (*continued*)

| Name | CHP | MGH | DZD | ALC | YXP |
|---|---|---|---|---|---|
| Isopentenyl pyrophosphate | 1.22E+06 ± 1.19E+06 | 1.22E+10 ± 8.89E+09 | 9.78E+08 ± 8.14E+08 | 8.24E+07 ± 1.15E+07 | 4.17E+06 ± 2.89E+06 |
| Glufosinate | 1.44E+08 ± 3.52E+07 | 2.67E+08 ± 1.46E+08 | 1.59E+08 ± 1.25E+08 | 2.77E+06 ± 8.86E+05 | 5.56E+06 ± 2.30E+06 |
| Iminodiacetic acid | 3.87E+07 ± 1.20E+07 | 1.04E+08 ± 3.27E+07 | 2.18E+08 ± 7.35E+07 | 9.22E+08 ± 3.17E+07 | 3.45E+08 ± 4.29E+07 |
| D-gluconate | 1.08E+08 ± 4.64E+07 | 5.53E+07 ± 1.08E+07 | 4.84E+07 ± 3.38E+07 | 7.52E+07 ± 1.66E+07 | 5.47E+09 ± 1.74E+09 |
| Daidzein | 3.11E+05 ± 7.74E+04 | 2.51E+08 ± 3.40E+07 | 6.96E+05 ± 4.47E+05 | 3.31E+05 ± 9.51E+04 | 1.25E+06 ± 8.89E+05 |
| Allantoin | 3.84E+08 ± 1.11E+08 | 1.06E+09 ± 3.51E+08 | 2.07E+09 ± 6.77E+08 | 9.14E+09 ± 1.28E+09 | 3.26E+09 ± 4.34E+08 |
| 1-naphthoic acid | 3.88E+06 ± 8.03E+05 | 2.83E+06 ± 7.97E+05 | 1.86E+06 ± 7.44E+05 | 3.42E+06 ± 5.46E+05 | 4.32E+07 ± 1.27E+07 |
| 4.alpha.-mannobiose | 1.06E+06 ± 6.67E+05 | 1.66E+08 ± 7.86E+07 | 1.31E+07 ± 9.68E+06 | 1.29E+07 ± 3.52E+06 | 4.61E+05 ± 2.33E+05 |
| 1-stearoyl-2-hydroxy-sn-glycero-3-phosphate | 1.16E+06 ± 6.12E+05 | 5.36E+06 ± 3.38E+06 | 1.75E+08 ± 1.84E+07 | 3.40E+05 ± 1.70E+05 | 3.78E+06 ± 1.89E+06 |
| 2,2′-methylene-bis(6-tert-butyl)-4-ethylphenol | 3.96E+09 ± 1.62E+09 | 2.04E+09 ± 1.13E+09 | 2.26E+07 ± 1.59E+07 | 1.18E+09 ± 3.16E+08 | 5.76E+08 ± 2.27E+08 |
| *N*-acetylneuraminate | 9.67E+07 ± 1.33E+07 | 1.97E+07 ± 6.97E+06 | 5.36E+07 ± 3.36E+07 | 1.07E+08 ± 9.85E+06 | 6.37E+08 ± 1.19E+08 |
| Citraconic acid | 6.74E+07 ± 5.36E+06 | 6.96E+07 ± 5.38E+06 | 4.88E+07 ± 6.60E+06 | 2.01E+08 ± 4.68E+07 | 2.70E+08 ± 6.97E+07 |
| Erythritol | 1.91E+05 ± 7.94E+04 | 5.16E+07 ± 3.63E+07 | 3.49E+06 ± 3.81E+06 | 3.65E+05 ± 1.69E+05 | 2.00E+08 ± 1.72E+07 |
| Taurine | 1.85E+09 ± 4.36E+08 | 1.67E+08 ± 7.00E+07 | 1.92E+08 ± 8.82E+07 | 1.51E+08 ± 1.88E+07 | 2.42E+09 ± 1.14E+09 |
| Inosine | 3.19E+07 ± 2.22E+07 | 3.05E+08 ± 1.77E+08 | 9.91E+07 ± 1.12E+08 | 1.63E+09 ± 4.81E+08 | 2.68E+09 ± 7.45E+08 |
| D-Mannose | 1.48E+09 ± 2.95E+08 | 6.05E+08 ± 1.95E+08 | 7.35E+08 ± 3.24E+08 | 4.43E+08 ± 2.96E+07 | 4.44E+09 ± 7.73E+08 |
| D-mannitol | 1.51E+08 ± 2.08E+07 | 4.63E+07 ± 2.15E+07 | 8.02E+07 ± 2.01E+07 | 5.94E+07 ± 4.19E+06 | 2.71E+08 ± 5.87E+07 |
| Uridine | 4.25E+09 ± 4.12E+08 | 2.43E+10 ± 3.32E+09 | 4.14E+09 ± 3.86E+09 | 7.36E+09 ± 8.15E+08 | 3.45E+10 ± 8.33E+09 |
| Glucose | 8.35E+07 ± 8.41E+06 | 6.67E+07 ± 1.26E+07 | 6.64E+07 ± 1.14E+07 | 7.06E+07 ± 1.21E+07 | 1.59E+08 ± 4.28E+07 |
| L-Threonine | 9.63E+07 ± 1.59E+07 | 3.73E+08 ± 2.26E+08 | 8.93E+07 ± 1.28E+08 | 8.91E+06 ± 1.51E+06 | 1.19E+07 ± 3.95E+06 |
| Glutamic acid | 8.26E+09 ± 3.30E+09 | 7.51E+09 ± 1.42E+09 | 3.30E+09 ± 4.54E+09 | 8.64E+08 ± 9.95E+07 | 2.08E+08 ± 9.29E+07 |
| Sucrose | 1.19E+08 ± 1.11E+08 | 4.39E+08 ± 1.92E+08 | 4.05E+08 ± 3.60E+08 | 8.55E+07 ± 5.88E+06 | 8.25E+08 ± 5.02E+08 |
| L-Valine | 1.43E+08 ± 7.42E+07 | 3.55E+08 ± 2.56E+08 | 7.84E+07 ± 7.32E+07 | 1.46E+08 ± 2.26E+07 | 3.87E+07 ± 8.67E+06 |

### 3.3.2. *Subcellular localisation analysis*

An investigation into the subcellular localization of all expressed proteins was conducted, with the findings presented in Fig. 3B. The outcomes revealed comparable extracellular protein content among DZD, MGH, and ALC relative to CHP and YXP. Additionally, proteins within the cytoplasm predominantly exhibited localization within cell membrane structures, mitochondria, lysosomes, and the endoplasmic reticulum (ER**).**

### 3.3.3. *GO functional analysis*

The gene ontology (GO) terms were assigned and sequence annotations were performed using the Bblast2GO software. The GO annotation results were visualized using R scripts. As shown in Fig. 3C. The y-axis of the graph represents the GO Level 2 functional annotation information, which includes Biological Process (in blue), Molecular Function (in yellow), and Cellular Component (in pink). The x-axis represents the number of expressed proteins in each functional category.

### 3.3.4. *KEGG pathway analysis*

Using the KEGG Automatic Annotation Server (KAAS) software, the expressed proteins were annotated with Kyoto Encyclopedia of Genes and Genomes (KEGG) pathway information. As shown in Fig. 3D. The pathway with the highest number of expressed proteins in MGH and DZD is “Protein processing in endoplasmic reticulum”. For ALC, the pathway with the highest number of expressed proteins is “Endocytosis”.

### 3.3.5. *Network analysis*

Based on the protein-protein interaction data obtained from the STRING database (http://string-db.org/), the interaction relationships between differentially expressed proteins were determined. The top 100 proteins with the highest connectivity were selected, and the generated interaction network was analyzed using the CytoScape software (Version 3.2.1) to visualize the network graph. As shown in Fig. 3E, in most species, the proteins Albumin (ALB), Alpha-2-HS-glycoprotein (AHSG), Apolipoprotein H (APOH), Serpin Family C Member 1 (SERPINC1), Recombinant Glycocalicin (GC), Lactotransferrin (LTF), and Hemopexin (HPX) show strong interactions with other proteins. Among them, ALB has the highest number of interactions with other proteins such as CHP, ALC, and YXP.

### 3.3.6. *Common proteins screening*

As shown in Fig. 6, a total of 34 common proteins were screened from five species. Among them, human milk contains relatively high levels of receptor protein-tyrosine kinase and Galectin-3-binding protein. The fibrinogen beta chain and Monocyte differentiation antigen CD14 are present in relatively high abundance in ALC. YXP contains more aminopeptidase.

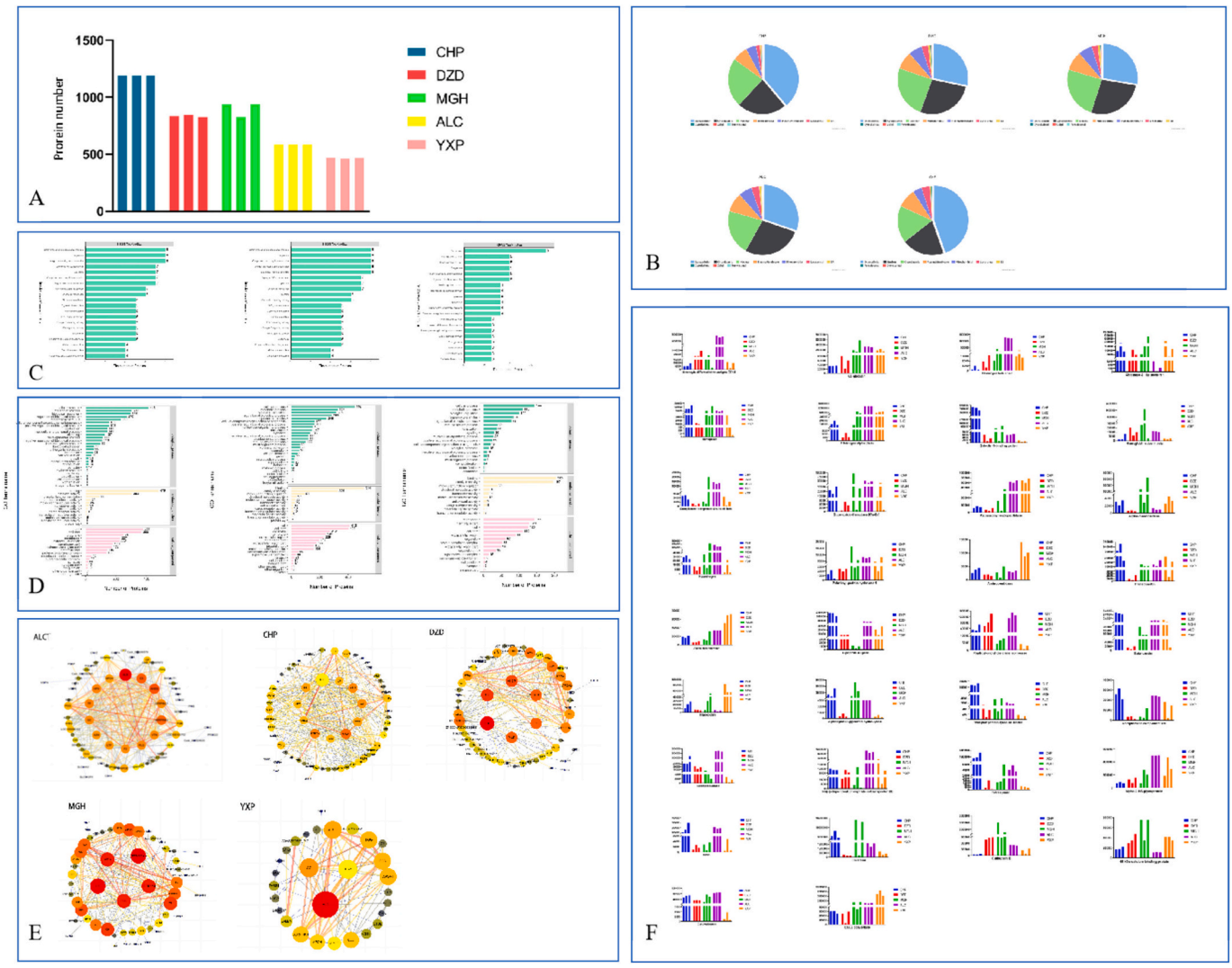


**Fig. 3.** (A) Histogram of protein; (B) Subcellular localisation analysis; (C) KEGG pathway; (D) GO Functional Analysis; (E) Interaction network analysis; (F) Common protein.

### *3.4. Integration analysis of metabolomics and proteomics*

#### *3.4.1. Correlation coefficient matrix Heatmap*

Fig. 4A illustrates the correlation between differentially expressed proteins and metabolites. The Pearson correlation coefficient value, denoted as r, ranges between −1 and + 1. A positive r indicates a positive correlation, shown in red, while a negative r indicates a negative correlation, depicted in blue. Darker colors signify stronger correlations. With the blue dashed line as the demarcation, the correlation coefficient matrix heatmap can be divided into four quadrants. The top-left quadrant displays the correlation among significantly different proteins, the bottom-right quadrant shows the correlation among significantly different metabolites, and both the top-right and bottom-left quadrants exhibit the correlation between significantly different proteins and metabolites, following a mirrored symmetry pattern.

#### *3.4.2. Hierarchical clustering Heatmap*

Fig. 4B presents the hierarchical clustering heatmap for differentially expressed proteins and metabolites. Clustering reveals that significantly different metabolites or proteins within the same cluster exhibit similar expression patterns. Each cell in the hierarchical clustering heatmap contains two pieces of information: the correlation coefficient r and the *p*-value. A positive r indicates a positive correlation, displayed in red, while a negative r is represented in blue. Darker colors indicate stronger correlations.

#### *3.4.3. Correlation network analysis*

Using Cytoscape software, significant differential proteins and metabolites obtained through Pearson correlation network analysis with coefficient values $|r| \geq 0.99$ as criteria were used to establish an interaction network graph between the proteome and metabolome. As shown in Fig. 4C, in the protein-metabolite interaction network graph of the DZD group, Beta-lactoglobulin-2 had the highest number of interacting connections with metabolites, interacting with 8 metabolites respectively. In the protein-metabolite interaction network graph of the MGH group, Ceruloplasmin had the highest number of interacting connections with metabolites, interacting with 5 metabolites respectively. In the protein-metabolite interaction network graph of the ALC group, the metabolite Trans-4-(aminomethyl)cyclohexanecarboxylic acid had the highest number of interacting connections with proteins, interacting with 4 metabolites respectively.

#### *3.4.4. Comparative analysis of KEGG pathway annotation*

Count the top 10 KEGG pathways with the highest number of proteins and metabolites co-involved and create a bar chart. As shown in Fig. 4D, the results of the DZD protein-metabolite pathway annotation

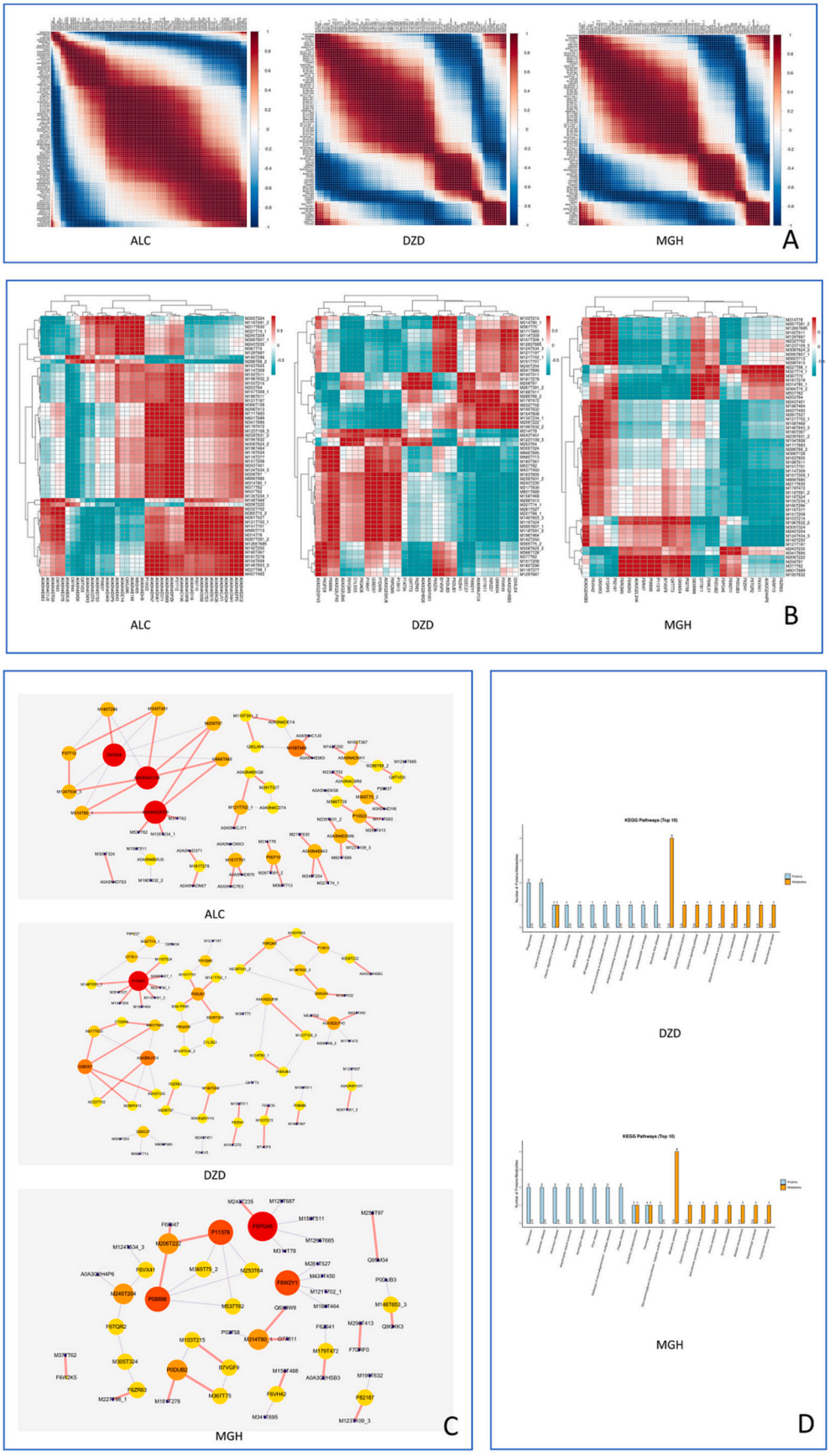


**Fig. 4.** Integration Analysis of Metabolomics and Proteomics (A) Correlation Coefficient Matrix Heatmap; (B) Hierarchical Clustering Heatmap; (C) Interaction network analysis; (D) KEGG Pathway.

analysis showed that the protein Apolipoprotein E and the metabolite niacinamide are jointly involved in the most pathways, specifically in the "Vitamin digestion and absorption" pathway. Similarly, the results of the MGH protein-metabolite pathway annotation analysis revealed that the protein ATP synthase subunit beta and the metabolite NADH are jointly involved in the most pathways, specifically in the "Oxidative Phosphorylation" and "Thermogenesis" pathways.

### 3.5. Integration analysis of proteomics and Lipidomic

#### 3.5.1. Correlation coefficient matrix Heatmap

Fig. 5A depicts the correlation between differentially Expressed Proteins and lipids. The value of the Pearson correlation coefficient, labeled as r, lies within the range from −1 to +1. A positive r implies a positive correlation, presented in red. A negative r suggests a negative correlation, represented in blue. Darker colors indicate more intense correlations.

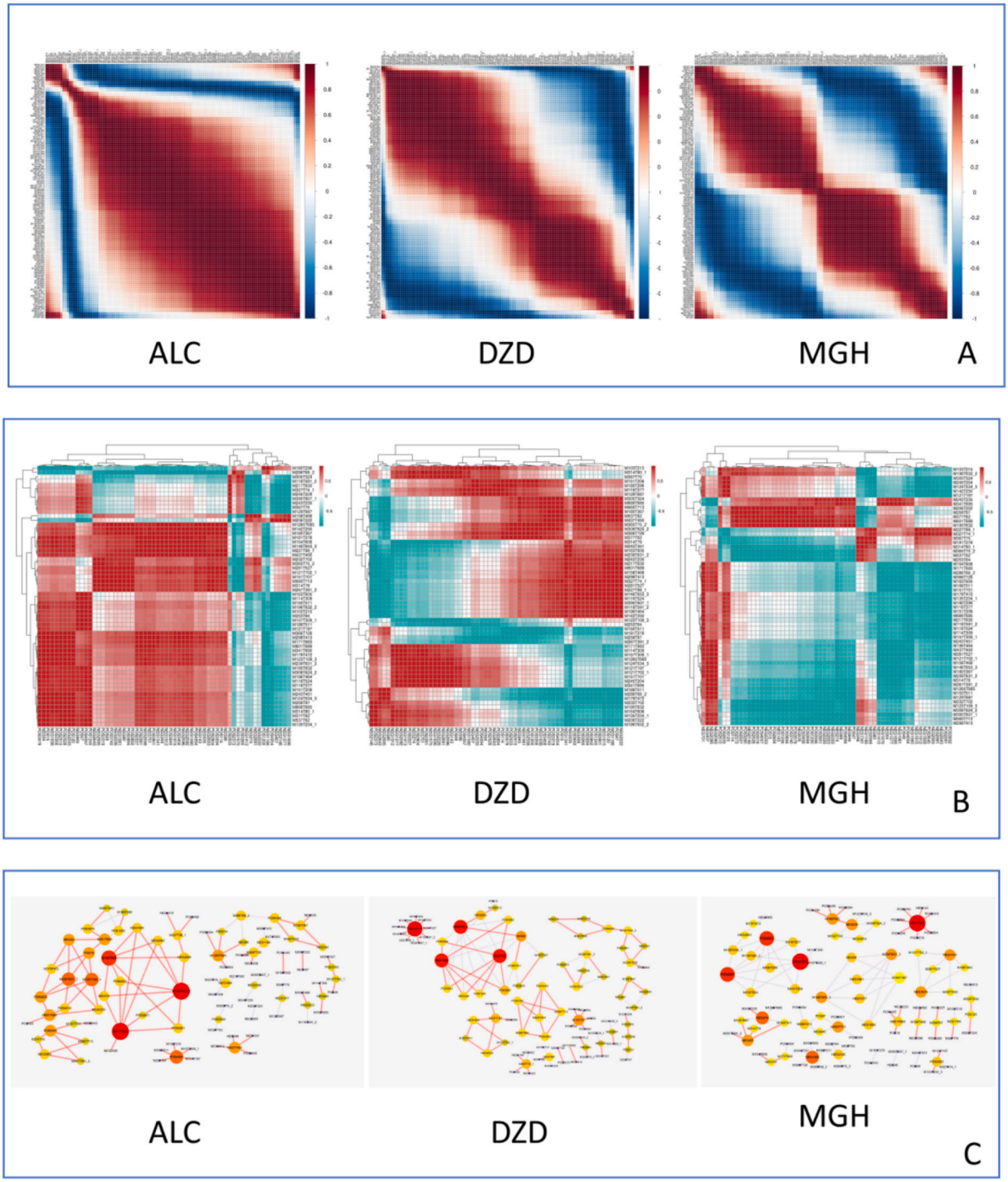


**Fig. 5.** Integration Analysis of Proteomics and Lipidomic (A) Correlation Coefficient Matrix Heatmap; (B) Hierarchical Clustering Heatmap; (C) Interaction network analysis.

#### 3.5.2. Hierarchical clustering Heatmap

Fig. 5B shows the hierarchical clustering heatmap of differentially expressed proteins and lipids. Through clustering, it is revealed that significantly different metabolites or lipids within the same cluster show similar expression patterns. Each cell in the hierarchical clustering heatmap contains two pieces of information: the correlation coefficient r and the *p*-value. A positive r indicates a positive correlation, presented in red, while a negative r is represented in blue. Darker colors signify stronger correlations.

#### 3.5.3. Correlation network analysis

Using the Cytoscape software, a significant interaction network between differentially expressed proteins and lipids was constructed based on the criteria of $|r| \geq 0.99$ obtained from Pearson correlation network analysis. As shown in Fig. 5C, in the protein-lipid interaction network of the DZD group, Heat shock protein HSP 90-beta exhibited the highest number of interaction connections with lipid molecules, interacting with 8 lipid species. In the protein-lipid interaction network of the MGH group, Butyrophilin subfamily 1 member A1 and Polymeric immunoglobulin receptor had the most interaction connections with lipid molecules, each interacting with 6 lipid species. In the protein-lipid interaction network of the ALC group, Carboxypeptidase D showed the highest number of interaction connections with lipid molecules, interacting with 6 lipid species.

### 3.6. Integration analysis of metabolomics and Lipidomic

#### 3.6.1. Correlation coefficient matrix Heatmap

Fig. 6A illustrates the correlation between differentially expressed metabolites and lipids.

#### 3.6.2. Hierarchical clustering Heatmap

Fig. 6B presents the hierarchical clustering heatmap for differentially expressed metabolites and lipids.

#### 3.6.3. Correlation network analysis

Using the Cytoscape software, a significant interaction network between differentially expressed metabolites and lipids was constructed based on the criteria of $|r| \geq 0.99$ obtained from Pearson correlation network analysis. As shown in Fig. 6C, in the metabolite-lipid interaction network of the DZD group, Tenofovir、1-stearoyl-2-hydroxy-sn-glycero-3-phosphateexhibited and Phe(benzoyl)-leu-arg exhibited the highest number of interaction connections with lipid molecules, interacting with 8 lipid species. In the metabolite-lipid interaction network of the MGH group, 4.alpha.-mannobiose had the most interaction connections with lipid molecules, each interacting with 7 lipid species. In the metabolite-lipid interaction network of the ALC group, glutamic acid and D-mannitol showed the highest number of interaction connections with lipid molecules, interacting with 7 lipid species.

## 4. Discussion

In different species of milk, there are inter-species differences in the distribution of total lipids and lipid subclasses. As shown in Fig. 1B, the total lipid content is higher in ALC compared to DZD and MGH (including CHP and YXP), which is consistent with previous studies (Zhao, Zhang, Ge, & Wang, 2022). As shown in Fig. 1B, there are significant differences in the distribution of lipid subclasses between ALC and other species, while DZD and MGH have similar distributions of lipid subclasses, which may be related to the different digestive systems of ruminant animals. Ruminant animals have a unique digestive organ called the rumen, which contains a diverse array of prokaryotic and eukaryotic microorganisms. These microorganisms rapidly convert plant biomass into short-chain fatty acids (SCFA) (Weimer & Kohn, 2016) and utilize lignocellulosic material to convert non-protein nitrogen into microbial protein for energy and amino acids (Newbold & Ramos-Morales, 2020). Regulation of the rumen environment can modify the fatty acid (FA) intake of mammary lipids and subsequently alter the composition of milk lipids (Toral, Monahan, Hervás, Frutos, & Moloney, 2018). Ruminant animals primarily consume plant-based feed, which is characterized by high fiber and low carbohydrates, and often harbors microbial populations. These microorganisms may also influence the conversion of fatty acids. For example, certain probiotic lactobacilli have the ability to convert linoleic acid (LA) to conjugated linoleic acid (CLA) (Aziz et al., 2023). In contrast, monogastric animals such as DZD and MGH have less diverse microbial communities in their gastrointestinal tracts compared to ALC. This may explain the higher lipid content in ALC and the differences in lipid subclass distribution among the three species.

As shown in Table 1, compared to CHP and YXP, MGH has higher abundance of TG and DG. ALC contains more PL. Studies have indicated that camel milk fat globules contain a significant amount of PL compared to human milk fat globules and bovine milk fat globules. However, the PL content in camel milk has not received much attention. The major phospholipids found in the milk fat globule membrane of camel milk are PC, PE, SM, PI, and PS (Bakry et al., 2021). This supports the observation that ALC has a higher abundance of phospholipids. Currently, this study has discovered the high abundance of TG and DG in MGH, but there is no research confirming this, thus further research and experiments are needed.

In this study, the screened differential metabolites were classified into Organoheterocyclic compounds, Organic acids and derivatives, benzenoids, alkaloids and derivatives, organic oxygen compounds, lipids and lipid-like molecules, and phenylpropanoids and polyketides. Xanthurenic acid, a metabolite of the canine uric acid pathway (KP). Research has shown that xanthurenic acid can affect brain function and neurotransmission, and interact with the metabotropic glutamate (mGlu) receptors. Xanthurenic acid has potential implications in the treatment of psychiatric disorders and is a promising candidate as a peripheral biomarker for such diseases (Fazio et al., 2017; Taleb, Maammar, Klein, Maitre, & Mensah-Nyagan, 2021). However, in this study, we found that xanthurenic acid is highly expressed in DZD. This suggests that DZD may have a therapeutic effect on mental disorders. Among the differentially expressed metabolites highly expressed in MGH, acridinone is an important heterocyclic scaffold, with both synthetic derivatives and natural derivatives holding significant biological value. Over the past decade, natural and synthetic compounds of the acridinone family have demonstrated antimicrobial and antitumor activities, with some derivatives being selected for antibacterial or anticancer chemotherapy (Mohammadi-Khanaposhtani et al., 2015). This indicates that MGH may have antibacterial and anti-inflammatory effects, which is consistent with previous studies (Musaev et al., 2021). Gabapentin and l-valine both belong to the category of organic acids and derivatives. Gabapentin exerts its effects by modulating neurotransmission and inhibiting excitatory neurons, commonly used to treat epilepsy, neuropathic pain, and pain resulting from other neurological disorders (Ladich, Zhou, Spence, & Moore, 2022). L-valine is widely used in various products such as food, pharmaceuticals, and animal feed (Wang, Zhang, & Quinn, 2018). Although research on the therapeutic aspects of l-valine in diseases is limited, a study found that administering l-valine to ischemic rats could alleviate arrhythmias and lower blood pressure (Mitręga et al., 2011). Gabapentin and l-valine are highly expressed in MGH, suggesting potential roles in analgesia and blood pressure modulation. In MGH, another differential metabolite with high expression levels and analgesic properties, ethylmorphine. Ethylmorphine, is a common opiate component found in cough suppressants. Its molecular structure is similar to morphine, with the only difference being the addition of an ethyl group at the 3 position. A derivative of ethylmorphine, ethylmorphine hydrochloride (EtM), is a potent analgesic and antitussive medication that, in the liver, is metabolized to morphine by ethylmorphine-*N*-demethylase. Its action involves blocking the transmission of pain signals to the brain to relieve pain, making it

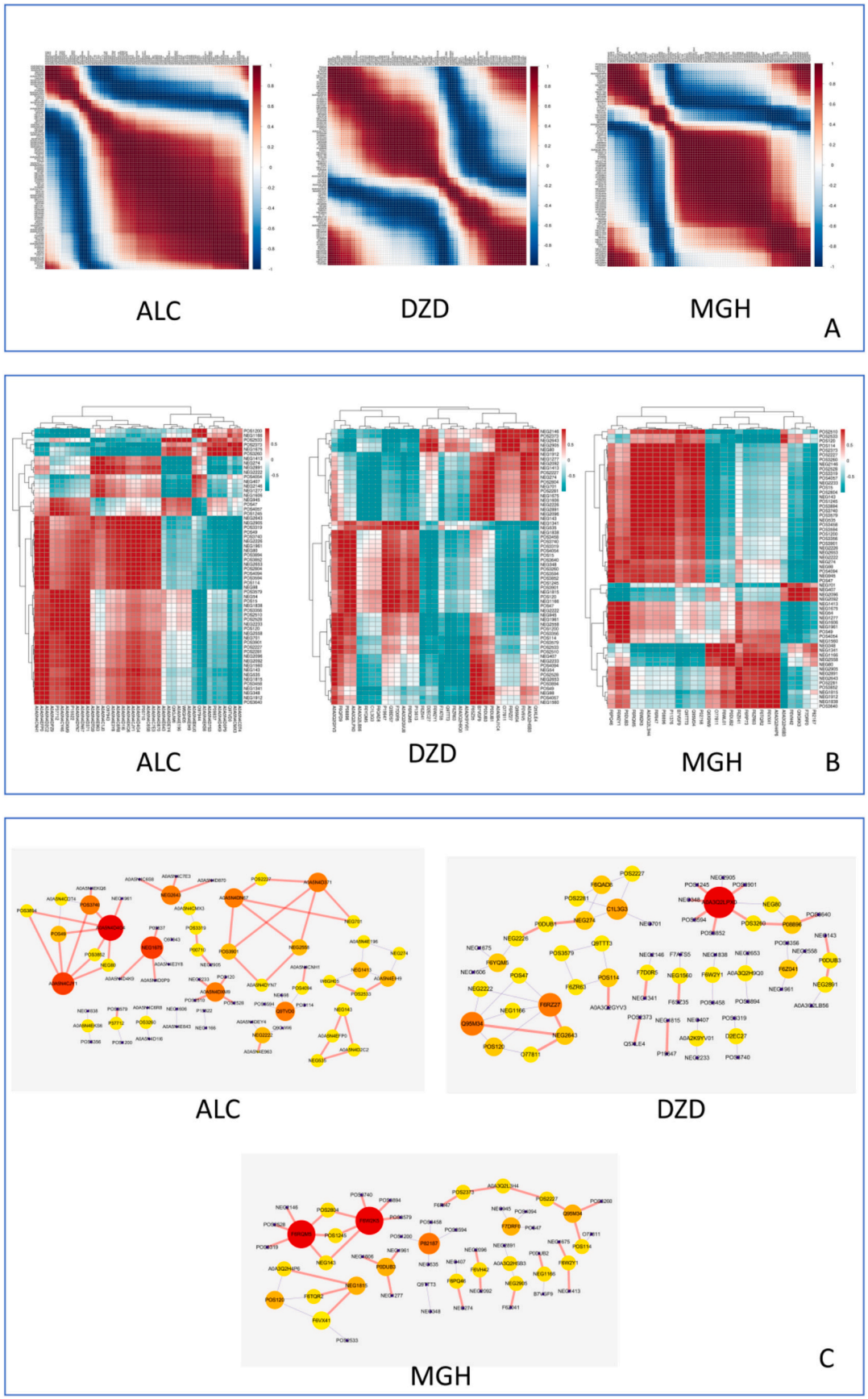


**Fig. 6.** Integration Analysis of Metabolomics and Lipidomic (A) Correlation Coefficient Matrix Heatmap; (B) Hierarchical Clustering Heatmap; (C) Interaction network analysis.

useful not only for severe pain associated with bone and cancer but also for alleviating muscle spasms and cramps (ElMeshad, Abdel-Haleem, Abdel Gawad, El-Nabarawi, & Sheta, 2020). The high expression of ethylmorphine in MGH further supports the potential role of MGH in pain relief. Erythritol is a natural sweetener produced endogenously through the pentose phosphate pathway (PPP). It is approximately 30 % less sweet than sucrose, with negligible calories. As a sugar substitute, it is widely used in low-calorie foods, confectionery, or baked goods. Research suggests that the biological function of erythritol is not just as a sugar substitute but that it exerts positive protective effects on the oral cavity compared to sugar, and its unique metabolic pathway is friendly to diabetic patients. In this study, the high expression levels of erythritol in MGH suggest that MGH could be a good choice for maintaining oral health and for diabetic patients (Baeza et al., 2020). And another differentially expressed metabolite within MGH: daidzein. Daidzein is a naturally occurring compound that belongs to the category of phenolpropanoids and polyketides. Some studies have shown that daidzein has beneficial effects on cardiovascular health, cholesterol reduction, anti fibrosis and anti diabetes (Jia et al., 2023). These studies suggest that MGH may be more suitable for people with diabetes. Chronic pain often leads to anxiety and depression, and studies have shown that ethosuximide can reduce nociception in chronic pain mouse models, improving anxiety- and depression-like behaviors. This suggests that ethosuximide may have some anxiolytic and antidepressant effects (Kerckhove et al., 2019). In ALC, another differentially expressed metabolite with high levels is l-deprenyl. L-deprenyl, also known as selegiline, is a type B monoamine oxidase (MAO-B) inhibitor that prevents the action of the dopamine-degrading enzyme, thereby maintaining dopamine levels in the nigrostriatal pathway. This maintenance of dopamine levels forms the basis for the use of l-deprenyl in the treatment of Parkinson's disease (Ryu et al., 2018). Although the exact mechanism of l-deprenyl's anti-apoptotic activity is not fully understood, it is believed to exert its neuroprotective effects by regulating the expression of antioxidant enzymes and anti-apoptotic genes, as well as preserving mitochondrial function (Abdanipour, Nikfar, Nikbakht Rad, Jafari Anarkooli, & Mansouri, 2022). This suggests that ALC may have neuroprotective effects. Furthermore, existing studies have shown that ALC can alleviate anxiety and depression (Khatoon, Ikram, & Abbas, 2019).

As shown in Fig. 3E, ALB (albumin) emerges as a central protein with the highest degree and coexpression in the PPI networks of CHP, ALC and YXP milk. ALB is the major protein in plasma and primarily an extravascular protein in all species. It plays a crucial role in the homeostasis of the endothelium. Albumin has numerous functions, including maintaining colloid osmotic pressure, promoting wound healing, reducing oxidative damage, etc. Its ability to bind to various compounds allows it to clear drugs, transport endogenous substances, and participate in clotting (Bihari, Bannard-Smith, & Bellomo, 2020). It can be imagined that ALB plays a multifaceted role in immune regulation, lipid metabolism, antioxidant activity, and nutrient transport, possibly synergizing with other proteins.

As Fig. 3F illustrated, CHP contains higher levels of receptor protein-tyrosine kinase (RPTK) and galectin-3-binding protein (LG3BP) compared to other species. RPTKs are a class of transmembrane proteins that play a critical role in cell signaling, regulating physiological processes such as cell growth, differentiation, and migration (Siever & Verderame, 1994). While the growth factors typically discussed in human milk, such as epidermal growth factor (EGF), are not directly referred to as RPTKs, the growth factors present can bind to cell surface RPTKs, triggering signaling pathways that promote cell proliferation, differentiation, and survival—crucial for infant development (Cohen, 1983). For example, EGF and similar growth factors aid in skin and mucosal repair, support intestinal epithelial health (Miller & Debas, 1995; Qi, Yang, Zhu, & Chen, 2019), enhance gut barrier function, and reduce infection risk (Rowland, Choi, & Warner, 2013). Notable members of the RPTK family include epidermal growth factor receptor (EGFR), Ffibroblast growth factor receptor (FGFR), and vascular endothelial growth factor receptor (VEGFR), many of which are implicated in cancer progression and serve as targets for anti-cancer drugs (Kissau, Stahl, Mazitschek, Giannis, & Waldmann, 2003; Nakamura et al., 2021; Roskoski, 2020). LG3BP is a multifunctional glycoprotein that can bind to galectin-3 and various other ligands. Galectin-3, as a β-galactoside-binding lectin, plays a role in inflammation, immune response and tumor progression (Fortuna-Costa, Gomes, Kozlowski, Stelling, & Pavão, 2014; Radosavljevic et al., 2012). LG3BP regulates its function through interaction with Galectin-3 and may affect the release of apoptosis and inflammatory mediators (Nielsen, Østergaard, Rasmussen, Jacobsen, & Heegaard, 2017). LG3BP plays a crucial role in regulating immune responses, coping with inflammation and resisting infections. Studies have shown that LG3BP has both intracellular and extracellular innate immune functions and has a significant stimulating effect on the activity of natural killer cells and lymphokine-activated killer cells in the immune defense system. In addition, LG3BP can combine with tumor necrosis factor receptor-associated factor 6 (TRAF6) and tumor necrosis factor receptor-associated factor 3 (TRAF3) complexes to produce interferon (IFN) and pro-inflammatory substances (Natoli, Iacobelli, & Kohn, 1996; Xu et al., 2019). However, its specific role in the innate immune response triggered by virus infection has not been clearly determined. It is worth mentioning that LG3BP present in human milk is regarded as having a protective effect on acute respiratory infections in infants and shows significant immune efficacy (Fornarini et al., 1999). Although RPTK is not directly present in breast milk but indirectly promotes physical growth through interaction with growth factors in breast milk. LG3BP, as one of the components of breast milk, may affect physical growth and development through multiple channels. These two proteins work synergistically through different mechanisms to promote human health. As can be seen from Fig. 3E, compared with other species, the contents of CD14 and the β-chain of fibrinogen in ALC are higher. As a product of camels, the nutritional components in camel milk may have a certain connection with the environmental adaptability of camels. Monocyte differentiation antigen CD14 (CD14) is a membrane protein widely distributed on the surfaces of monocytes and macrophages, playing a key role in innate immunity. As a cell surface receptor, CD14 can recognize and bind to pathogen-associated molecular patterns (PAMPs), and it has a particularly high affinity for lipopolysaccharide (LPS), which is an important component of the cell wall of Gram-negative bacteria. After CD14 binds to LPS, it activates a specific signaling pathway, triggering the production of pro-inflammatory cytokines and initiating an immune response. (Sharygin, Koniaris, Wells, Zimmers, & Hamidi, 2023). In addition, CD14 is not only directly involved in the immune response. It also plays a key role in immune regulation and can effectively help control the degree of inflammatory response (Ciesielska, Matyjek, & Kwiatkowska, 2021). It has been found through research that the mo-II monocyte subset with CD14high MHCIIhigh in camels exhibits significant inflammatory characteristics, indicating a close correlation between the high expression of CD14 and inflammatory functions. In harsh environments densely populated with pathogens, such as deserts, the high expression of CD14 in camel milk may help the young camels rapidly establish an immune defense system. Meanwhile, the number of cells in this subset in the peripheral blood of newborn camel calves is significantly lower than that in adult individuals, suggesting that the expression level of CD14 is closely related to the growth and development stages of camels (Hussen et al., 2020). The β-chain of fibrinogen, as a key component of blood coagulation, plays an important role in wound repair. When blood vessels are damaged, fibrinogen is converted into fibrin under the action of thrombin, forming a physical barrier to stop bleeding. In addition, its degradation products can participate in the processes of cell adhesion and migration, thereby promoting wound healing (Laurens, Koolwijk, & de Maat, 2006; Simurda et al., 2020). In the desert environment, camels face a higher risk of injury. The high expression of the β-chain of fibrinogen in camel milk provides an abundant material basis for wound repair, which helps to reduce the risk of infection and increase the

survival rate. Although CD14 and the β-chain of fibrinogen have different functions, they work in concert within the body's defense mechanism. The former eliminates pathogens through immune responses, while the latter forms a physical barrier through the blood coagulation process. There is a significant interaction between the two: the inflammatory response mediated by CD14 can enhance the permeability of blood vessels, promote the release of coagulation factors, and accelerate the blood coagulation process (Verbon et al., 2003). In turn, the fibrin network formed during the blood coagulation process can capture pathogens and prevent the spread of infection (Esmon, Xu, & Lupu, 2011). These findings suggest that the high expression of CD14 and the β-chain of fibrinogen in camel milk may be closely related to the unique environmental adaptability of camels, and these related proteins may have evolved special functions to adapt to extreme environments. However, the specific mechanisms of action of these proteins in camels still require further in-depth research. Aminopeptidase is a class of enzymes whose function is to remove amino acids one by one from the amino end (N-terminus) of proteins or polypeptide chains. Aminopeptidase participates in protein metabolism and is very important for the digestion and absorption of proteins (Mucha, Drag, Dalton, & Kafarski, 2010). In pig milk, there may be specific enzymes, including but not limited to aminopeptidase. These enzymes may be involved in the preliminary processing of proteins in milk and help piglets better digest and absorb the nutritional components in milk. For example, some aminopeptidases may help break down larger protein molecules into smaller peptide segments, thereby improving the digestion efficiency of piglets. When studying the nutritional value of pig milk and the digestive physiology of piglets, understanding the enzyme activity in milk is very important.

In the pathway annotation results of protein-metabolite correlation analysis, we identified an important differential metabolite, niacinamide. Niacinamide (NAM) is the water-soluble form of vitamin B3 (niacin) and is also the precursor of nicotinamide adenine dinucleotide ($NAD^+$), which regulates cellular energy metabolism and plays a role in the production of adenosine triphosphate (ATP) (Nikas, Paschou, & Ryu, 2020). $NAD^+$ is a biological hydride acceptor that can form the reduced form of the dinucleotide, NADH. The $NAD^+$/NADH dinucleotide drives various oxidation-reduction reactions in cellular energy metabolism and provides electrons for aerobic ATP production. NADH plays a crucial role in energy metabolism, but excessive levels of NADH can be toxic. When there is insufficient oxygen in the cell or the oxygen cannot be effectively utilized, NADH accumulates (Yang et al., 2020). $NAD^+$ plays a crucial role in the body, directly and indirectly influencing many key cellular functions including metabolic pathways, DNA repair, chromatin remodeling, cell aging, and immune cell function (Covarrubias, Perrone, Grozio, & Verdin, 2021). It is worth noting that the levels of $NAD^+$ gradually decrease with age. The decline in $NAD^+$ levels is causally related to many age-related diseases, including cognitive decline, cancer, metabolic disorders, muscle wasting, and frailty. Many age-related diseases can be slowed down or even reversed by restoring $NAD^+$ levels (Wu et al., 2023). Niacinamide exhibits high expression levels in DZD, and research has demonstrated that DZD possesses antioxidant, anti-aging, and antimicrobial properties, as well as potential effects in alleviating some inflammation-related chronic diseases (Li et al., 2020). This may be related to the role of niacinamide in energy metabolism.

## 5. Conclusion

This study employed omics techniques to conduct in-depth investigations of donkey milk, mare milk, and camel milk. The research results show that compared with DZD and MGH, the phospholipid content in ALC is higher. In MGH, the differentially expressed metabolites with high expression levels include acridinone, xanthurenic acid, nicotinamide, gabapentin, L-valine, ethylmorphine, erythritol, and daidzein. In ALC, there are high levels of L-deprenyl and ethosuximide. In addition, human milk contains more receptor protein-tyrosine kinase and galectin-3-binding protein; camel milk contains more CD14 and fibrinogen beta chain; and pig milk contains more aminopeptidase. However, this study has certain limitations, including the lack of verification of functional substances. Therefore, future research should focus on clarifying the functional effects among related substances.

The informed consent statement obtained for this study.

In this study, we are committed to ensuring that the rights and autonomy of all individuals participating in the research are fully protected. When recruiting subjects, we introduced the specific contents of the research to them in clear and understandable language, including the research process, possible risks and expected benefits. The animal experiments involved in this study all followed the relevant animal welfare and ethical guidelines. Before the experiment began, we elaborated on the design and operation process of the experiment to the animal keepers and managers in detail to ensure that they understood and agreed to the conduct of the experiment.

## Author contribution

The authors' contributions were as follows: Qiu Zhang, Qian Li, Xiaowei Wang, Zeying Wang: designed the research; Zeying Wang, Qiu Zhang, Qian Li, Xiaowwei Wang: wrote the manuscript; Yanzhi Wu, Rui Chen, Yinggang Sun: performed the systematic literature search, screened publications for eligibility; Yuan Pan, Siyi Li: extracted the data and scored the study quality; Zeying Wang: Conceptualization; Writing—review and editing; All authors: interpreted the results, had responsibility for the final content, and read and approved the final manuscript.

## CRediT authorship contribution statement

**Qiu Zhang:** Formal analysis, Data curation. **Qian Li:** Formal analysis, Data curation, Conceptualization. **Xiaowei Wang:** Software, Resources. **Yanzhi Wu:** Supervision, Software. **Rui Chen:** Supervision, Software. **Yinggang Sun:** Methodology, Investigation. **Yuan Pan:** Visualization, Supervision, Software. **Siyi Li:** Validation, Supervision. **Zeying Wang:** Data curation, Conceptualization.

## Declaration of competing interest

The authors declare the following financial interests/personal relationships which may be considered as potential competing interests: Zeying wang reports article publishing charges was provided by Shenyang Agricultural University. If there are other authors, they declare that they have no known competing financial interests or personal relationships that could have appeared to influence the work reported in this paper.

## Acknowledgement

We are very grateful to Dr. Zeying Wang for all the help he gave us in completing the research article, as well as the funding from the postdoctoral science foundation of China [2021M693859].

## Data availability

Data will be made available on request.

## References

Abdanipour, A., Nikfar, A., Nikbakht Rad, M., Jafari Anarkooli, I., & Mansouri, M. (2022). Neuroprotective effect of L-deprenyl on the expression level of the Mst1 gene and inhibition of apoptosis in rat-model spinal cord injury. *Iranian Journal of Basic Medical Sciences, 25*(1), 53–59. https://doi.org/10.22038/ijbms.2022.58031.12894

Aziz, T., Naveed, M., Shabbir, M. A., Sarwar, A., Ali Khan, A., Zhennai, Y., & Alasmari, A. F. (2023). Comparative genomics of food-derived probiotic Lactiplantibacillus plantarum K25 reveals its hidden potential, compactness, and

efficiency. *Frontiers in Microbiology, 14*, 1214478. https://doi.org/10.3389/fmicb.2023.1214478
Baeza, M., Morales, A., Cisterna, C., Cavalla, F., Jara, G., Isamitt, Y., & Gamonal, J. (2020). Effect of periodontal treatment in patients with periodontitis and diabetes: Systematic review and meta-analysis. *Journal of Applied Oral Science, 28*, Article e20190248. https://doi.org/10.1590/1678-7757-2019-0248
Bakry, I. A., Yang, L., Farag, M. A., Korma, S. A., Khalifa, I., Cacciotti, I., & Wang, X. (2021). A comprehensive review of the composition. In *Nutritional value, and functional properties of camel Milk fat. Foods (Basel, Switzerland), Vol. 10(9)*. https://doi.org/10.3390/foods10092158
Bihari, S., Bannard-Smith, J., & Bellomo, R. (2020). Albumin as a drug: Its biological effects beyond volume expansion. *Critical care and resuscitation : journal of the Australasian Academy of Critical Care Medicine, 22*(3), 257–265. https://doi.org/10.1016/s1441-2772(23)00394-0
Ciesielska, A., Matyjek, M., & Kwiatkowska, K. (2021). TLR4 and CD14 trafficking and its influence on LPS-induced pro-inflammatory signaling. *Cellular and Molecular Life Sciences, 78*(4), 1233–1261. https://doi.org/10.1007/s00018-020-03656-y
Cohen, S. (1983). The epidermal growth factor (EGF). *Cancer, 51*(10), 1787–1791. https://doi.org/10.1002/1097-0142(19830515)51:10<1787::aid-cncr2820511004>3.0.co;2-a
Covarrubias, A. J., Perrone, R., Grozio, A., & Verdin, E. (2021). NAD(+) metabolism and its roles in cellular processes during ageing. *Nature Reviews. Molecular Cell Biology, 22*(2), 119–141. https://doi.org/10.1038/s41580-020-00313-x
Damen, C. W. N., Isaac, G., Langridge, J., et al. (2014). Enhanced lipid isomer separation in human plasma using reversed-phase UPLC with ion-mobility/high-resolution MS detection. *Journal of Lipid Research, 55*(8), 1772–1783. https://doi.org/10.1194/jlr.D047795
ElMeshad, A. N., Abdel-Haleem, K. M., Abdel Gawad, N. A., El-Nabarawi, M. A., & Sheta, N. M. (2020). Core in cup Ethylmorphine hydrochloride tablet for dual fast and sustained pain relief: Formulation, characterization, and pharmacokinetic study. *AAPS PharmSciTech, 21*(7), 244. https://doi.org/10.1208/s12249-020-01759-0
Esmon, C. T., Xu, J. X., & Lupu, F. (2011). Innate immunity and coagulation. *Journal of Thrombosis & Haemostasis, 9*(Supplement s1), 182–188. https://doi.org/10.1111/j.1538-7836.2011.04323.x
Fazio, F., Lionetto, L., Curto, M., Iacovelli, L., Copeland, C. S., Neale, S. A., & Nicoletti, F. (2017). Cinnabarinic acid and xanthurenic acid: Two kynurenine metabolites that interact with metabotropic glutamate receptors. *Neuropharmacology, 112*(Pt B), 365–372. https://doi.org/10.1016/j.neuropharm.2016.06.020
Fornarini, B., Iacobelli, S., Tinari, N., Natoli, C., De Martino, M., & Sabatino, G. (1999). Human milk 90K (mac-2 BP): Possible protective effects against acute respiratory infections. *Clinical and Experimental Immunology, 115*(1), 91–94. https://doi.org/10.1046/j.1365-2249.1999.00782.x
Fortuna-Costa, A., Gomes, A. M., Kozlowski, E. O., Stelling, M. P., & Pavão, M. S. (2014). Extracellular galectin-3 in tumor progression and metastasis. *Frontiers in Oncology, 4*, 138. https://doi.org/10.3389/fonc.2014.00138
Hsu, Y. J., Jhang, W. L., Lee, M. C., Bat-Otgon, B., Narantungalag, E., & Huang, C. C. (2021). Lactose-riched Mongolian mare's milk improves physical fatigue and exercise performance in mice. *International Journal of Medical Sciences, 18*(2), 564–574. https://doi.org/10.7150/ijms.53098
Hussen, J., Shawaf, T., Al-Mubarak, A. I. A., Humam, N. A. A., Almathen, F., & Schuberth, H. J. (2020). Dromedary camel cd14high mhciihigh monocytes display inflammatory properties and are reduced in newborn camel calves. *BMC Veterinary Research, 16*. https://doi.org/10.1186/s12917-020-02285-8
Ji, Z., Zhang, J., Deng, C., Hu, Z., Du, Q., Guo, T., & Yang, Y. (2023). Identification of mare milk adulteration with cow milk by liquid chromatography-high resolution mass spectrometry based on proteomics and metabolomics approaches. *Food Chemistry, 405*(Pt B), Article 134901. https://doi.org/10.1016/j.foodchem.2022.134901
Jia, J., He, R., Yao, Z., Su, J., Deng, S., Chen, K., & Yu, B. (2023). Daidzein alleviates osteoporosis by promoting osteogenesis and angiogenesis coupling. *PeerJ, 11*, Article e16121. https://doi.org/10.7717/peerj.16121
Kerckhove, N., Boudieu, L., Ourties, G., Bourdier, J., Daulhac, L., Eschalier, A., & Mallet, C. (2019). Ethosuximide improves chronic pain-induced anxiety- and depression-like behaviors. *European neuropsychopharmacology : the journal of the European College of Neuropsychopharmacology, 29*(12), 1419–1432. https://doi.org/10.1016/j.euroneuro.2019.10.012
Khatoon, H., Ikram, R., & Abbas, G. (2019). Neuropharmacological effects of camel milk related to modulation of biogenic amines in experimental animals. *Pakistan Journal of Pharmaceutical Sciences, 32*(6), 2633–2641.
Kissau, L., Stahl, P., Mazitschek, R., Giannis, A., & Waldmann, H. (2003). Development of natural product-derived receptor tyrosine kinase inhibitors based on conservation of protein domain fold. *Journal of Medicinal Chemistry, 46*(14), 2917–2931. https://doi.org/10.1021/jm0307943
Ladich, E. M., Zhou, K. Q., Spence, D. L., & Moore, C. B. (2022). Opioid-sparing anesthesia: Gabapentin and postoperative pain. *Journal of perianesthesia nursing : official journal of the American Society of PeriAnesthesia Nurses, 37*(6), 966–970. https://doi.org/10.1016/j.jopan.2022.04.008
Laurens, N., Koolwijk, P., & de Maat, M. P. (2006). Fibrin structure and wound healing. *Journal of Thrombosis and Haemostasis, 4*(5), 932–939. https://doi.org/10.1111/j.1538-7836.2006.01861.x
Li, Y., Fan, Y., Shaikh, A. S., Wang, Z., Wang, D., & Tan, H. (2020). Dezhou donkey (Equus asinus) milk a potential treatment strategy for type 2 diabetes. *Journal of Ethnopharmacology, 246*, Article 112221. https://doi.org/10.1016/j.jep.2019.112221
Li, Y., Ma, Q., Liu, G., & Wang, C. (2022). Effects of donkey milk on oxidative stress and inflammatory response. *Journal of Food Biochemistry, 46*(4), Article e13935. https://doi.org/10.1111/jfbc.13935
Miller, C. A., & Debas, H. T. (1995). Epidermal growth factor stimulates the restitution of rat gastric mucosa in vitro. *Experimental Physiology, 80*(6), 1009–1018. https://doi.org/10.1113/expphysiol.1995.sp003898
Mitręga, K., Zorniak, M., Varghese, B., Lange, D., Nożynski, J., Porc, M., & Krzemiński, T. F. (2011). Beneficial effects of l-leucine and l-valine on arrhythmias, hemodynamics and myocardial morphology in rats. *Pharmacological Research, 64*(3), 218–225. https://doi.org/10.1016/j.phrs.2011.04.011
Mohamed, H., Johansson, M., Lundh, Å., Nagy, P., & Kamal-Eldin, A. (2020). Short communication: Caseins and α-lactalbumin content of camel milk (Camelus dromedarius) determined by capillary electrophoresis. *Journal of Dairy Science, 103*(12), 11094–11099. https://doi.org/10.3168/jds.2020-19122
Mohammadi-Khanaposhtani, M., Safavi, M., Sabourian, R., Mahdavi, M., Pordeli, M., Saeedi, M., & Akbarzadeh, T. (2015). Design, synthesis, in vitro cytotoxic activity evaluation, and apoptosis-induction study of new 9(10H)-acridinone-1,2,3-triazoles. *Molecular Diversity, 19*(4), 787–795. https://doi.org/10.1007/s11030-015-9616-0
Mucha, A., Drag, M., Dalton, J. P., & Kafarski, P. (2010). Metallo-aminopeptidase inhibitors. *Biochimie, 92*(11), 1509–1529. https://doi.org/10.1016/j.biochi.2010.04.026
Musaev, A., Sadykova, S., Anambayeva, A., Saizhanova, M., Balkanay, G., & Kolbaev, M. (2021). Mare's Milk: Composition, properties, and application in medicine. *Archives of Razi Institute, 76*(4), 1125–1135. https://doi.org/10.22092/ari.2021.355834.1725
Nakamura, I. T., Kohsaka, S., Ikegami, M., Ikeuchi, H., Ueno, T., Li, K., & Mano, H. (2021). Comprehensive functional evaluation of variants of fibroblast growth factor receptor genes in cancer. *npj Precision Oncology, 5*(1), 66. https://doi.org/10.1038/s41698-021-00204-0
Natoli, C., Iacobelli, S., & Kohn, L. (1996). The immune stimulatory protein 90K increases major histocompatibility complex class I expression in a human breast cancer cell line. *Biochemical and Biophysical Research Communications, 225*(2), 617–620. https://doi.org/10.1006/bbrc.1996.1219
Newbold, C. J., & Ramos-Morales, E. (2020). Review: Ruminal microbiome and microbial metabolome: Effects of diet and ruminant host. *Animal : an international journal of animal bioscience, 14*(S1), s78–s86. https://doi.org/10.1017/s1751731119003252
Nie, S., Zhao, Y., Qiu, X., Wang, W., Yao, Y., Yi, M., & Wang, D. (2019). Metabolomic study on nude mice models of gastric Cancer treated with modified Si Jun Zi Tang via HILIC UHPLC-Q-TOF/MS analysis. *Evidence-based Complementary and Alternative Medicine, 2019*, 3817879. https://doi.org/10.1155/2019/3817879
Nielsen, C. T., Østergaard, O., Rasmussen, N. S., Jacobsen, S., & Heegaard, N. H. H. (2017). A review of studies of the proteomes of circulating microparticles: Key roles for galectin-3-binding protein-expressing microparticles in vascular diseases and systemic lupus erythematosus. *Clinical Proteomics, 14*, 11. https://doi.org/10.1186/s12014-017-9146-0
Nikas, I. P., Paschou, S. A., & Ryu, H. S. (2020). The role of nicotinamide in Cancer chemoprevention and therapy. *Biomolecules, 10*(3). https://doi.org/10.3390/biom10030477
Qi, S., Yang, C., Zhu, M., & Chen, H. (2019). Effect of oral mucosal transplantation on the expression of EGF and VEGF-C during skin wound repair. *Experimental and Therapeutic Medicine, 18*(1), 320–325. https://doi.org/10.3892/etm.2019.7546
Radosavljevic, G., Volarevic, V., Jovanovic, I., Milovanovic, M., Pejnovic, N., Arsenijevic, N., & Lukic, M. L. (2012). The roles of Galectin-3 in autoimmunity and tumor progression. *Immunologic Research, 52*(1–2), 100–110. https://doi.org/10.1007/s12026-012-8286-6
Roskoski, R. (2020). The role of fibroblast growth factor receptor (FGFR) protein-tyrosine kinase inhibitors in the treatment of cancers including those of the urinary bladder. *Pharmacological Research, 151*, Article 104567. https://doi.org/10.1016/j.phrs.2019.104567
Rowland, K. J., Choi, P. M., & Warner, B. W. (2013). The role of growth factors in intestinal regeneration and repair in necrotizing enterocolitis. *Seminars in Pediatric Surgery, 22*(2), 101–111. https://doi.org/10.1053/j.sempedsurg.2013.01.007
Ryu, I., Ryu, M. J., Han, J., Kim, S. J., Lee, M. J., Ju, X., & Kweon, G. R. (2018). L-Deprenyl exerts cytotoxicity towards acute myeloid leukemia through inhibition of mitochondrial respiration. *Oncology Reports, 40*(6), 3869–3878. https://doi.org/10.3892/or.2018.6753
Sharygin, D., Koniaris, L. G., Wells, C., Zimmers, T. A., & Hamidi, T. (2023). Role of CD14 in human disease. *Immunology, 169*(3), 260–270. https://doi.org/10.1111/imm.13634
Siever, D. A., & Verderame, M. F. (1994). Identification of a complete Cek7 receptor protein tyrosine kinase coding sequence and cDNAs of alternatively spliced transcripts. *Gene, 148*(2), 219–226. https://doi.org/10.1016/0378-1119(94)90692-0
Simurda, T., Brunclikova, M., Asselta, R., Caccia, S., Zolkova, J., Kolkova, Z., & Kubisz, P. (2020). Genetic variants in the FGB and FGG genes mapping in the Beta and Gamma nodules of the fibrinogen molecule in congenital quantitative fibrinogen disorders associated with a thrombotic phenotype. *International Journal of Molecular Sciences, 21*(13). https://doi.org/10.3390/ijms21134616
Suo, L., Liang, X., Zhang, W., et al. (2024). Potential prognostic biomarkers of hepatocellular carcinoma based on 4D label-free quantitative proteomics analysis: Pilot investigation. *International Journal of Biological Markers, 39*(1). https://doi.org/10.1177/03936155231212925
Taleb, O., Maammar, M., Klein, C., Maitre, M., & Mensah-Nyagan, A. G. (2021). A role for Xanthurenic acid in the control of brain dopaminergic activity. *International Journal of Molecular Sciences, 22*(13). https://doi.org/10.3390/ijms22136974

Toral, P. G., Monahan, F. J., Hervás, G., Frutos, P., & Moloney, A. P. (2018). Review: Modulating ruminal lipid metabolism to improve the fatty acid composition of meat and milk. *Challenges and opportunities. Animal : an international journal of animal bioscience, 12*(s2), s272–s281. https://doi.org/10.1017/s1751731118001994

Verbon, A., Meijers, J. C. M., Spek, C. A., Hack, C. E., Pribble, J. P., Turner, T., … van der Poll, T. (2003). Effects of IC14, an anti - CD14 antibody, on coagulation and fibrinolysis during low - grade Endotoxemia in humans. *The Journal of Infectious Diseases, 187*(1), 55–61. https://doi.org/10.1086/346043

Wang, X., Zhang, H., & Quinn, P. J. (2018). Production of L-valine from metabolically engineered Corynebacterium glutamicum. *Applied Microbiology and Biotechnology, 102*(10), 4319–4330. https://doi.org/10.1007/s00253-018-8952-2

Weimer, P. J., & Kohn, R. A. (2016). Impacts of ruminal microorganisms on the production of fuels: How can we intercede from the outside? *Applied Microbiology and Biotechnology, 100*(8), 3389–3398. https://doi.org/10.1007/s00253-016-7358-2

Wu, W., Yuan, S., Tang, Y., Meng, X., Peng, M., Hu, Z., & Liu, W. (2023). Effect of exercise and Oral Niacinamide mononucleotide on improving mitochondrial autophagy in Alzheimer's disease. *Nutrients, 15*(13). https://doi.org/10.3390/nu15132851

Wu, Y., Sun, Y., Chen, R., Qiao, Y., Zhang, Q., Li, Q., & Wang, Z. (2023). Analysis for lipid nutrient differences in the milk of 13 species from a quantitative non-targeted lipidomics perspective. *Food Chem X, 20*, Article 101024. https://doi.org/10.1016/j.fochx.2023.101024

Xu, G., Xia, Z., Deng, F., Liu, L., Wang, Q., Yu, Y., & Liu, S. (2019). Inducible LGALS3BP/90K activates antiviral innate immune responses by targeting TRAF6 and TRAF3 complex. *PLoS Pathogens, 15*(8), Article e1008002. https://doi.org/10.1371/journal.ppat.1008002

Yang, L., Garcia Canaveras, J. C., Chen, Z., Wang, L., Liang, L., Jang, C., & Rabinowitz, J. D. (2020). Serine catabolism feeds NADH when respiration is impaired. *Cell Metabolism, 31*(4), 809–821.e806. https://doi.org/10.1016/j.cmet.2020.02.017

Zhang, X., Li, H., Yu, J., Zhou, X., Ji, C., Wu, S., & Zhao, F. (2019). Label-free based comparative proteomic analysis of whey proteins between different milk yields of Dezhou donkey. *Biochemical and Biophysical Research Communications, 508*(1), 237–242.

Zhao, L., Zhang, J., Ge, W., & Wang, J. (2022). Comparative Lipidomics analysis of human and ruminant Milk reveals variation in composition and structural characteristics. *Journal of Agricultural and Food Chemistry, 70*(29), 8994–9006. https://doi.org/10.1021/acs.jafc.2c02122

Zhao, Y., Yu, S., Zhao, H., Li, L., Li, Y., Tu, Y., Jiang, L., & Zhao, G. (2022). Lipidomic profiling using GC and LC-MS/MS revealed the improved milk quality and lipid composition in dairy cows supplemented with citrus peel extract. *Food research international (Ottawa, Ont.), 161*, Article 111767. https://doi.org/10.1016/j.foodres.2022.111767